

Links between foreland rheology and the growth and evolution of a young mountain belt in New Guinea

Lizzie Knight^{1*}, Alex Copley¹, Claudia Bertoni², Alistair Sloan³, and Richard Walker²

¹COMET, Bullard Laboratories, Department of Earth Sciences, University of Cambridge, UK

²Department of Earth Sciences, University of Oxford, UK

³Department of Geological Sciences, University of Cape Town, South Africa

*epk26@cam.ac.uk

Accepted XX/XX/XXXX; Received XX/XX/XXXX; In original form XX/XX/XXXX

Abbreviated title: Foreland rheology and mountain range evolution in New Guinea

Summary

We have studied the active and recent tectonics of New Guinea, using earthquake source modelling, analysis of gravity anomalies, seismic reflection profiles, and thermal and mechanical models. Our aim is to investigate the behaviour and evolution of a young continental deformation belt, and to explore the effects of lateral variations in foreland rheology on the deformation. We find that along-strike gradients in the lithosphere thickness of the southern foreland have resulted in correlated changes in seismogenic thickness, likely due to the effects on the temperature structure of the crust. The resulting variation in the strength of the foreland means that in the east, the foreland is broken through on thrust faults, whereas in the west it is relatively intact. The lack of correlation between the elevation of the mountain belt and the seismogenic thickness of the foreland is likely to be due to the time taken to thicken the crust in the mountains following changes in the rheology of the underthrusting foreland, as the thinned passive margin of northern Australia is consumed. The along-strike variation in whether the force exerted between the mountains and the lowlands is able to break the foreland crust enables us to estimate the effective coefficient of friction on foreland faults to be in the range of 0.01-0.28. We use force-balance calculations to show that the recent tectonic re-organisation in western New Guinea is likely to be due to the development of increasing curvature in the Banda Arc, and that the impingement of continental material on the subduction zone may explain the unusually low force it exerts on western New Guinea.

Keywords: Neotectonics, Rheology: crust and lithosphere, Rheology and friction of fault zones, Earthquake source observations, Continental margins: convergent, Seismicity and tectonics

1 Introduction

1 The rheology of continental lithosphere – and its controls on tectonic deformation – has long
2 been the source of debate. Discussion has surrounded the distribution of strength in continental
3 lithosphere, and rheological differences between Precambrian cratons and younger intervening de-
4 formation belts (e.g. Chen and Molnar, 1983; Maggi et al., 2000b; Townend and Zoback, 2000;
5 Burov and Watts, 2006; Jackson et al., 2008; Burov, 2010). One of the main methods that has
6 been used to estimate the strength of the lithosphere is based upon observations and models of
7 active mountain ranges and their forelands. The distribution of strain within the ranges can be
8 used to estimate the material properties of the mountain belt, and flexure and earthquakes in
9 the bounding forelands can be used to infer their rheology (e.g. Dalmayrac and Molnar, 1981;
10 England and Houseman, 1989; England and Molnar, 2015). However, most of this previous work
11 has focused on relatively long-lived mountain belts like Tibet and the Andes, in which the foreland
12 now adjacent to the ranges represents the former continental interior of the bounding plates. In
13 order to fully explore the degree, and causes, of lateral variability in continental rheology, it is
14 therefore important to investigate immature collision zones, where the foreland at least partially
15 represents the continental margin of the bounding plate.

16

17 For this reason, we have chosen to study New Guinea, where the laterally-variable continental
18 margin of the northern Australian Plate forms the southern foreland to the deformation belt. This
19 mountain range – the New Guinea Highlands – is the product of a young, active arc-continent col-
20 lision, caused by rapid oblique convergence between the Australian and Pacific Plates (presently
21 110 mm/yr; DeMets et al., 1994). The orogeny is thought to have begun in the mid-Miocene
22 (Hill and Hall, 2003; Cloos et al., 2005), and the underthrusting Australian foreland displays large
23 pre-existing structural variations along-strike. Thus New Guinea provides an ideal opportunity to
24 study how along-strike variations in the mechanical properties and rheology of the lithosphere can
25 affect the early stages of mountain-building.

26

27 In this paper, we use seismological modelling techniques to determine accurate source param-
28 eters for recent earthquakes in central and western New Guinea. We combine these data with
29 elastic and thermal modelling to study along-strike rheological variation in the New Guinea High-
30 lands and southern foreland basin. Using additional geodetic and seismic reflection data, we also
31 explore the tectonic configuration and evolution of the region west of the mountains, where the
32 deformation pattern has switched from regional compression to extension over the last 2 My. We
33 make new estimates of the forces acting between the central mountains and forelands and estimate
34 the frictional strength of active foreland faults. We suggest how along-strike variations in foreland
35 lithospheric strength and mountain elevation may be related to each other, and explore the impli-
36 cations for the factors controlling the deformation in the early stages of mountain building. We
37 also investigate how changing plate-driving forces in southeast Asia have controlled the tectonic
38 evolution of western New Guinea through the late Cenozoic.

39

40 We begin by summarising the geological history and current tectonic setting of the region. We
41 then present newly-constrained estimates of depths and focal mechanisms of earthquakes in New
42 Guinea, before investigating lithosphere strength within the mountains and forelands. We then
43 describe new evidence for recent and active extension in western New Guinea. We reconcile our
44 observations with models of the lateral variations in the rheology of the lithosphere, and discuss
45 how the New Guinea Highlands may be expected to evolve over time. Finally, we discuss how
46 large-scale tectonic changes in the wider Indonesian region may have affected the tectonics of
47 western New Guinea.

2 Geological history and tectonic setting

2.1 Geology of New Guinea

New Guinea is situated on the northern edge of the Australian Plate. The island's geology reveals a complicated tectonic history of subduction, obduction, arc-continent collision, and mountain-building, driven by rapid oblique convergence between the Australian and Pacific Plates.

New Guinea has often been described as resembling a bird flying west (Moore, 2003). The island is thus divided geographically into (from west to east): the Bird's Head, Neck, Body, and Tail. Central New Guinea, or the Bird's Body, can itself be divided into three major WNW-ESE trending provinces (Figure 1C): the Southern Lowlands, a stable platform which marks the northern extent of the Australian Plate; the New Guinea Highlands, formed primarily of passive margin sediments which have been folded and thrust to form mountains with an average elevation of 2–3 km; and the Mobile Belt, a northern accretionary complex of ophiolites, metamorphic rocks, sediments, and island arc volcanics (Abers and McCaffrey, 1988; Nash et al., 1993; Hill and Hall, 2003; Baldwin et al., 2012).

The Southern Lowlands are comprised of Australian continental crust and form the foreland to the New Guinea Highlands. The Lowlands are divided by the Tasman Line (Figure 1B), a boundary which separates Proterozoic cratonic basement of the Australian Shield in the west from the Paleozoic Tasman Orogen in the east (Schiebner, 1974; Hamilton, 1979; Plumb, 1979). The Tasman Line approximately follows the Indonesia-Papua New Guinea border, but its location north of the Lowlands is poorly known (Hill and Hall, 2003). The Tasman Line is also roughly coincident with a change in lithosphere thickness observed in both New Guinea and Australia, such that the lithosphere is up to 100 km thicker to the west of the Tasman Line (Priestley et al., 2018; and discussed in more detail below).

In western New Guinea, the Bird's Head, Bird's Neck, and Cenderawasih Bay comprise the

75 Bird's Head Block, a region of Paleozoic basement overlain and intruded by basin sediments,
76 granitic intrusions, accreted arc material, and high grade metamorphics (Pieters et al., 1983;
77 Bailly et al., 2009; Jost et al., 2018). Eastern Papua New Guinea hosts the accreted Finisterre Arc
78 (Davies et al., 1997; Hill and Raza, 1999), and extensive ophiolite belts and arc magmatism along
79 the Papuan Peninsula (Davies and Jaques, 1984; Baldwin et al., 2012; Davies, 2012).

80 **2.2 Geological history**

81 During the Paleozoic, westwards subduction along the eastern margin of Australia (which was then
82 part of Gondwana) led to terrane accretion above the subduction zone and the development of the
83 Tasman Orogen, which was thrust westwards over the stable Precambrian craton which now forms
84 western Australia and New Guinea (Crawford et al., 2003; Glen, 2005). North-south rifting along
85 the northern Australian margin in the Mesozoic lead to the truncation of the Tasman Orogen and
86 the development of a passive margin up to 1,000 km wide across what is now New Guinea (Pigram
87 and Symonds, 1991; Veevers et al., 1991; Cloos et al., 2005).

88
89 Major tectonic change occurred in the early Eocene after the breakup of Gondwana, when the
90 Australian Plate drifted northwards as it separated from Antarctica (Royer and Sandwell, 1989;
91 Hall, 2002). Pacific lithosphere was subducted beneath the north and east sides of the Australian
92 passive margin, developing a volcanic island arc (Hill and Hall, 2003). Around 30 Ma, the arrange-
93 ment of the plate margins changed such that oceanic Australian lithosphere from the northern
94 passive margin began subducting northwards beneath the volcanic arc (Cloos et al., 2005). North-
95 wards subduction of the Australian Plate also occurred in the early Miocene beneath the Solomon
96 Sea (Webb et al., 2014).

97
98 Subduction of the Australian Plate ceased between 15-12 Ma, when Australian continental
99 crust reached the collision zone, and crustal shortening and orogenesis was initiated across Central
100 New Guinea (Visser and Hermes, 1962; Pigram et al., 1989; Pigram and Symonds, 1991; Cloos
101 et al., 2005; Webb et al., 2014). The New Guinea Highlands were formed primarily of deformation

102 of sediments from the passive margin and accretionary prism. North of the orogeny, the Mobile
103 Belt was developed as terranes from the volcanic arc and forearc basin, containing ophiolites,
104 metamorphic rocks, intrusives, and sediments, were accreted to the northern Australian margin
105 (Hamilton, 1979; Nash et al., 1993; Davies et al., 1997). The mid-Miocene also saw the active Java
106 subduction zone propagate eastwards through Indonesia and begin to subduct an embayment of
107 Indian oceanic crust from the western edge of Australian continent, initiating subduction along
108 the Banda Arc (Spakman and Hall, 2010; Figure 1B).

109

110 In the late Miocene, Pacific lithosphere began to subduct southwards beneath the north coast
111 of New Guinea (Tregoning and Gorbatov, 2004). Orogenic deformation and sedimentary deposi-
112 tion propagated rapidly southwards from the Mobile Belt into the southern fold-and-thrust belt
113 (Pigram and Symonds, 1991; Hill and Raza, 1999). Trench-parallel strike-slip activity occurred
114 along shear zones in western and central New Guinea (Dow and Sukamto, 1984; Cloos et al., 2005;
115 Bailly et al., 2009), whilst shortening remained dominant in the east (Hill and Hall, 2003).

116

117 In the late Miocene and Pliocene, northwards subduction of oceanic lithosphere in Cender-
118 awasih Bay led to collision between the Bird's Neck and the Weyland Overthrust, which formed the
119 Lengguru Fold-Thrust Belt (Figure 1B; Dow and Sukamto, 1984; Hill and Hall, 2003; de Sigoyer
120 et al., 2011, François et al., 2016). From the Pliocene onwards, compression waned across the
121 central New Guinea Highlands, as strike-slip tectonics became dominant at high elevation and
122 thrusting migrated to the presently-active thrust front on the southern edge of the range (Abers
123 and McCaffrey, 1988; Cloos et al., 2005). Pliocene and Quaternary volcanism has been identified
124 within the Highlands, though its origin is debated (e.g. Johnson et al., 1978; Hamilton et al.,
125 1983; McDowell et al., 1996; Cloos et al., 2005). The most recent major tectonic change occurred
126 around 2 Ma when the Bird's Neck and Cenderawasih Bay became a region of transtension, with
127 deformation taken up along the edges of the bay and the Tarera-Aiduna Fault (Pubellier and Ego,
128 2002; Bailly et al., 2009).

129 **2.3 Present tectonic setting**

130 At present, the broad-scale tectonics of central New Guinea are driven by oblique convergence
131 between the Australian and Pacific Plates, which occurs at a rate of 110 mm/yr along an azimuth
132 of 248° (Figure 1A; DeMets et al., 1994). The convergence is oblique to the trend of major geo-
133 logical structures in central New Guinea (Figure 1B) and has been partitioned into ~ 70 mm/yr
134 of shortening and ~ 85 mm/yr of left-lateral shear across these structures (Dow and Sukamto,
135 1984; Abers and McCaffrey, 1988; Puntodewo et al., 1994; McCaffrey, 1996; Tregoning and Gor-
136 batov, 2004). GPS and seismic data suggest that between 10-60 mm/yr of the shortening may
137 be accommodated by subduction off the north coast at the New Guinea Trench, which produces
138 occasional megathrust earthquakes such as the M_w 8.2 earthquake on February 2nd 1996 (Mc-
139 Caffrey, 1996; Stevens et al., 2002; Tregoning and Gorbatoov, 2004). The remaining shortening
140 across the central part of the island is taken up on thrust faults within the New Guinea Highlands
141 and Mamberamo Basin (McCaffrey and Abers, 1988; Puntodewo et al., 1994; Wallace et al., 2004).

142
143 Central and western New Guinea is dominated by left-lateral strike-slip tectonics. Along the
144 north coast of the island, a semi-continuous shear zone runs sub-parallel to the New Guinea Trench.
145 From west to east, this shear zone is divided into the Sorong, Yapen, and Bewani-Torricelli Fault
146 Zones (Figure 1B). The shear zone exhibits a varying slip rate along-strike: GPS data reveal the
147 Yapen Fault Zone to be slipping at up to 46 mm/yr (Bock et al., 2003), while the Sorong Fault Zone
148 may slip at ~ 20 mm/yr west of 131°E but is mostly inactive where it outcrops on land (Puntodewo
149 et al., 1994; Stevens et al., 2002). Accumulated offset along the Sorong and Yapen Fault Zones
150 is estimated between 370–900 km (Visser and Hermes, 1962; Dow and Sukamto, 1984; Charlton,
151 1996). The Tarera-Aiduna Fault, which lies south of Cenderawasih Bay and the Lengguru Fold-
152 Thrust Belt (Figure 1B), has an estimated left-lateral offset of 50 km (Hamilton et al., 1983) and
153 a slip rate of 20 mm/yr (McCaffrey and Abers, 1991). The Tarera-Aiduna Fault continues offshore
154 to the west where it meets the Seram Trench (Teas et al., 2009). Some left-lateral strain is also
155 taken up along the Paniai-Lowlands Fault Zone, which truncates the New Guinea Highlands on
156 the east side of Cenderawasih Bay. Faults within the Paniai-Lowlands Fault Zone display up to

157 1.5 km of vertical offset (Pubellier and Ego, 2002) and may accommodate ~ 20 mm/yr of extension
158 (Stevens et al., 2002), which suggests a transtensional nature to the fault zone.

159

160 Off the west coast of New Guinea, the Banda Arc represents an active collision between the
161 Australian continental margin and a volcanic arc (Carter et al., 1976; Hamilton, 1979; McCaf-
162 frey and Abers, 1991). Australian continental crust is being underthrust both northwards at the
163 Banda Trench and southwestwards at the Seram Trench, where the Bird's Head Block meets the
164 arc (Figure 1B). Deep seismicity implies that this continental material is connected to subducting
165 oceanic lithosphere at depth (McCaffrey, 1989). The tight curvature of the arc has sparked debate
166 regarding whether the collision involves deformation of a single continental slab at both trenches
167 (Hamilton, 1979; Spakman and Hall, 2010), or two separate slabs subducting towards each other
168 (Cardwell and Isacks, 1978; McCaffrey, 1989; Hinschberger et al., 2005).

169

170 In eastern Papua New Guinea, an active arc-continent collision is emplacing the Finisterre Arc
171 onto the northeast coast of the island along the Ramu-Markham Fault (Figure 1B), with maximum
172 convergence rates between 40-60 mm/yr (Davies et al., 1997; Wallace et al., 2004; Koulali et al.,
173 2015). Convergence continues along-strike at the New Britain Trench. The Owen-Stanley Fault
174 Zone on the Papuan Peninsula shows along-strike tectonic variability, transitioning from extension
175 at the southern tip, to oblique-sinistral slip which is exhuming a metamorphic core complex, to
176 shortening in the north where the fault zone meets the Ramu-Markham Fault (Wallace et al., 2004;
177 Daczko et al., 2011).

178

179 Within this overall context, we have chosen to study the active tectonics of the New Guinea
180 Highlands and southern foreland basin, as well as investigating active extension in the Bird's Neck
181 and Cenderawasih Bay. We will first describe new estimates of earthquake depths and mechanisms
182 in both regions, which we have made in order to study how variation in lithosphere properties may
183 be affecting the active tectonics. Our seismological methods are detailed in the following section.

3 Seismicity

3.1 Earthquake source parameter modelling

To study active deformation in central and western New Guinea, we have compiled a set of earthquakes which have been modelled to determine their source parameters, and have added to them 23 of our own analyses. Focal mechanisms and centroid depths determined by teleseismic body-waveform modelling were taken from the work of Abers and McCaffrey (1988) and Sloan and Jackson (2012). Of the new events analysed in this study, 14 events were studied using body-waveform modelling to determine depth, focal mechanism, magnitude, and source time function (Table 1), and 9 events were modelled using depth-phase analysis to estimate depth alone (Table 2). We chose to model these earthquakes in order to study the range of faulting styles in the southern foreland basin, New Guinea Highlands, and the Bird's Neck. While estimates of earthquake source parameters are available in online catalogues such as the gCMT (Dziewonski et al., 1981; Ekström et al., 2012) or ISC-EHB Bulletin (Weston et al., 2018; International Seismological Centre, 2020), the methods used in our study can significantly increase the accuracy of the source parameter estimates, in particular the centroid depth (Engdahl et al., 2006).

Teleseismic body-waveform modelling can be used for earthquakes of sufficient magnitude to result in good signal-to-noise ratio at teleseismic distances (typically $M_w \geq 5.4$) and with good azimuthal seismic station coverage. In this study, earthquake source parameters were determined using the MT5 program, which performs a joint inversion of P and SH seismic waveforms recorded at teleseismic distances (McCaffrey and Abers, 1988; McCaffrey et al., 1991; Zwick et al., 1994). The methodology behind this procedure has been extensively detailed in previous literature (e.g. Abers and McCaffrey, 1988; Molnar and Lyon-Caen, 1989; Taymaz et al., 1990) and need only be summarised here.

Broadband seismograms were downloaded from the IRIS DMC and deconvolved to reproduce the response of a long-period (15-100 s) WWSSN instrument. This process allows the earthquake

211 to be modelled as a point source and reduces sensitivity to small-scale heterogeneities in velocity
212 structure in the source region (Taymaz et al., 1990). For earthquakes within the foreland basin and
213 Bird’s Neck, we use a simple two-layer velocity model which represents an upper layer of sediments
214 ($V_p = 4.5$ km/s; $V_s = 2.7$ km/s; density = 2,400 kg/m³; layer thickness = 2 km) and a crustal
215 layer which hosts the earthquake source ($V_p = 6.5$ km/s; $V_s = 3.8$ km/s; density = 2,800 kg/m³).
216 Reasonable changes to the velocity structure alter earthquake source depth only within the limits
217 of expected uncertainties (± 4 km; Taymaz et al., 1990) and so the thickness of the upper sediment
218 layer was not altered for each individual event. For events in the Aru Trough, we use a water
219 layer with a thickness of 3.0–3.5 km (adjusted to match the observed water layer reverberations),
220 a sediment layer ($V_p = 3.0$ km/s; $V_s = 1.7$ km/s; density = 2,400 kg/m³; layer thickness = 5 km)
221 and a lower crustal layer ($V_p = 6.5$ km/s; $V_s = 3.8$ km/s; density = 2,800 kg/m³) (Jacobson et al.,
222 1979; Sloan and Jackson, 2012).

223

224 Seismic stations within 30–90° epicentral distance of the earthquake were selected in order to
225 avoid lithospheric reverberations and interactions with the core. Up to 50 P and SH seismograms
226 were selected after visual inspection of signal-to-noise ratio and to ensure sufficient azimuthal cov-
227 erage. The gCMT solution was then used as the starting model for the inversion, which minimises
228 the weighted least-squares misfit between the observed seismograms and synthetic seismograms
229 generated from the starting model. Seismograms were weighted by azimuthal density, and P
230 phases weighted by a factor of two compared to SH phases, to account for their lower amplitude.
231 The final solution was constrained to have a double-couple moment tensor. An example focal
232 mechanism produced using this method for the 15th November 2011 M_w 5.7 earthquake in the
233 New Guinea foreland is shown in Figure 2. The parameters of all earthquakes with new analyses
234 performed in this study are given in Table 1, and our inversion results for all events are displayed
235 in the supplemental information.

236

237 Uncertainties in the source parameters were estimated using the method of Taymaz et al.
238 (1990). Each source parameter was successively fixed and an inversion performed in which all

239 other source parameters were free to vary. The fixed parameter was varied sequentially on either
240 side of the minimum misfit value. The potential error was estimated by examining when the fit to
241 the observed waveforms was noticeably degraded. Errors in centroid depth were typically within
242 ± 5 km. Errors in focal mechanism were more variable and highly dependent on the azimuthal
243 distribution of seismic stations: strike errors were typically within $\pm 30^\circ$; dip errors within $\pm 15^\circ$;
244 and rake errors within $\pm 30^\circ$. For the 2nd February 2005 M_w 5.5 earthquake and the 5th Septem-
245 ber 2013 M_w 5.4 earthquake, the depth was well constrained by the MT5 program but the focal
246 mechanism was not, primarily due to poor seismic station coverage of the focal sphere. For these
247 two events, the gCMT focal mechanism solution was retained and we inverted only for centroid
248 depth, magnitude, and source time function.

249

250 For earthquakes of $M_w < 5.5$, or if azimuthal coverage was poor, or if there were few seis-
251 mic stations with an acceptable signal-to-noise ratio to allow inversion for the focal mechanism,
252 forward-modelling of depth phases was instead used to constrain the source depth of the event.
253 This method compares the P-wave and pP and sP near-source surface reflections between an ob-
254 served seismogram and a synthetic seismogram generated for a range of source depths, in order to
255 find the best-fitting depth. For each earthquake, broadband seismograms with visible depth phases
256 were selected, within the $30\text{--}90^\circ$ epicentral range. Synthetic seismograms were generated using the
257 WKB algorithm (Chapman et al., 1988), the ak135 global velocity model (Kennett et al., 1995),
258 and the gCMT focal mechanism (Dziewonski et al., 1981; Ekström et al., 2012). The observed P-
259 waves were aligned with the first arrival of their corresponding synthetic. The absolute amplitude
260 of the synthetic was scaled to fit the amplitude of the observed seismogram. By varying the source
261 depth used to calculate the synthetic waveforms, the best-fitting solution was selected via visual in-
262 spection of the synthetic and observed depth phases. Errors in source depth were typically ± 1 km.

263

264 For events we were unable to model ourselves due to limited data availability or quality, we
265 have used additional data from the gCMT catalogue and ISC-EHB Bulletin (Dziewonski et al.,
266 1981; Ekström et al., 2012; Weston et al., 2018; International Seismological Centre, 2020). A

merged earthquake catalogue was created, using gCMT focal mechanism solutions matched to events located by the ISC-EHB Bulletin; this was done because locations and depths located using the EHB algorithm are typically more accurate than those from the gCMT catalogue (Engdahl et al., 1998; Engdahl et al., 2006). The merged catalogue contains more than 4700 events of $M_w > 4.5$ which occurred between 1976-2016 across New Guinea.

3.2 Patterns of seismicity

The focal mechanisms of earthquakes modelled in this study and by Abers and McCaffrey (1988) and Sloan and Jackson (2012) are displayed in Figure 3, alongside the additional events from the gCMT catalogue. Figure 4 shows the location and depths of earthquakes across New Guinea, separated by focal mechanism.

The north coast of the New Guinea is dominated by shallow, left-lateral strike-slip earthquakes which are likely to be associated with the semi-continuous Sorong, Yapen, and Bewani-Torricelli Fault Zones, and reverse-faulting earthquakes associated with the New Guinea Trench; these reverse earthquakes generally have much greater magnitudes than the strike-slip events. There is also some strike-slip and reverse-faulting activity within the Mamberamo Basin.

Seismicity in northeast New Guinea is dominated by a major north-dipping subduction zone (the New Britain Arc) which runs from the northeast of the island offshore towards the island of New Britain. Deep earthquakes (> 60 km) beneath the northeast New Guinea Highlands are probably related to subduction along this arc. The strike-slip earthquakes concentrated along the northern coastline extend from the Bewani-Torricelli Fault Zone to the region north of the Bismarck Sea.

The overall pattern of seismicity in and around the New Guinea Highlands shows only a small amount of shallow crustal deformation presently occurring beneath the mountains (Figure 3 and Figure 4). The largest earthquakes in the region are strike-slip events, indicating that there is little

294 active crustal shortening within the range. The largest magnitude earthquakes are concentrated
295 beneath the western half of the Highlands. Earthquakes beneath the Highlands at depths greater
296 than ~ 60 km are likely associated with southwards subduction of the Pacific Plate at the New
297 Guinea Trench, instead of being associated with the orogeny. The southern range-front of the
298 Highlands is characterised by thrust-faulting earthquakes with nodal planes aligned approximately
299 parallel to the strike of the range front. These events tend to have nodal planes with dips $> 30^\circ$.
300 Our modelling techniques do not allow us to constrain which of the nodal planes is the fault plane,
301 though for these thrust-faulting events the fault plane is likely to be the north-dipping plane,
302 causing uplift in the fold-thrust belt and subsidence in the basin. South of the foreland basin, the
303 Southern Lowlands are mostly aseismic, with the exception of a small number of events that we
304 discuss in detail below.

305

306 To the west of the New Guinea Highlands, significant seismicity occurs within the Bird's Neck
307 and along the edges of Cenderawasih Bay. Where the Highlands meet the Bird's Neck, the region is
308 dominated by shallow strike-slip earthquakes, some of which are likely associated with the Tarera-
309 Aiduna Fault which continues westwards towards the Banda Arc. To the south of the Bird's Neck,
310 normal and strike-slip faulting is observed within the Aru Trough. The east side and north sides
311 of Cenderawasih Bay show mostly strike-slip earthquakes, whereas the west side is characterised
312 by shallow normal faulting. Seismic activity in the Bird's Head is concentrated along the north
313 coast and is associated with the Sorong Fault Zone and the New Guinea Trench.

314 4 New Guinea Highlands and forelands

315 We now examine in detail the New Guinea Highlands and their southern foreland, and combine our
316 estimated earthquake source parameters with thermal models and the analysis of gravity anomalies.

317 4.1 Earthquake depths and seismogenic thickness

318 Earthquake depths in the New Guinea Highlands and southern foreland basin, determined by
319 body-waveform modelling and depth-phase analysis, are shown in Figure 5, overlain on a map of
320 lithosphere thickness derived from surface wave tomography (Priestley et al., 2018). The vertical
321 resolution of the lithosphere thickness data is approximately 30 km, and the horizontal resolution
322 is between 250–400 km (Priestley et al., 2018). The deepest earthquakes (the 14th June 2016 M_w
323 5.2 event at 33 km depth in the foreland and the 2nd December 1982 M_w 5.5 event at 44 km depth
324 in the Highlands) occurred in the region of thickest lithosphere in New Guinea. The 1982 event
325 also occurred in the region where mountain elevation is highest.

326
327 We have used the modelled source depths of earthquakes to estimate the seismogenic thick-
328 ness (T_s) of the lithosphere: namely, the thickness of the brittle part of the lithosphere which
329 ruptures in earthquakes. For the magnitudes of the events we have studied (M_w 4.9–6.7), and for
330 commonly-observed displacement/length ratios (i.e. 5×10^{-5} ; Scholz, 1982), the rupture radius will
331 be on the order of 2–16 km. When combined with the fault dips determined in our inversion
332 analysis, the range of depth extents of the rupture patch are similar to, or smaller than, the depth
333 uncertainties from our inversion methods, and are small compared with the variations we describe
334 below. The earthquakes used to calculate seismogenic thickness in the foreland may not fully
335 represent the seismicity of the region, due to our limited observation time compared with the du-
336 ration of earthquake cycles. However, we have chosen not to supplement our data with earthquakes
337 from the gCMT or ISC-EHB catalogues (Dziewonski et al., 1981; Ekström et al., 2012; Interna-
338 tional Seismological Centre, 2020) as these catalogues provide less accurate depth estimates than
339 body-waveform modelling or depth-phase analysis (Engdahl et al., 2006). As such, our estimates

340 represent the minimum possible seismogenic thickness, given that future earthquakes may occur
341 at greater depths. However, we are encouraged in our approach by previous studies that have
342 established lateral variations in seismogenic thickness using similar numbers of earthquakes, which
343 have been confirmed by microseismic surveys and not contradicted by subsequent events (Chen
344 and Molnar, 1983; Chen and Molnar, 1990; Kayal and Zhao, 1998; Maggi et al., 2000a; Priestley
345 et al., 2008; Craig et al., 2011; Nissen et al., 2011; Sloan et al., 2011; Devlin et al., 2012; Nemati
346 et al., 2013; Craig and Jackson, 2021).

347

348 In the western foreland basin between 135–141°E, the seismogenic thickness is 33–36 km. This
349 estimate incorporates possible errors from our depth estimations, and uses the magnitudes of the
350 earthquakes to estimate a maximum possible depth of rupture from our estimated centroid depths
351 and magnitudes using a displacement/length ratio of 5×10^{-5} (Scholz, 1982; Figure 5C). We note
352 that the earthquake depths determined using depth-phase analysis represent hypocentres instead
353 of centroid depths, but the magnitude of these earthquakes is small ($< M_w$ 5.5) and so the max-
354 imum rupture depth is probably < 3 –4 km greater than the hypocentre depth. The seismogenic
355 thickness in this western region is consistent with the depths of earthquakes near the Aru Trough
356 on the western margin of the foreland (Sloan and Jackson, 2012; blue diamonds on Figure 5D).
357 Given that receiver function studies have estimated the crustal thickness of the northern Aus-
358 tralian shield, away from the edge of the plate, to be approximately 27–35 km (Jacobson et al.,
359 1979; Clitheroe et al., 2000), our estimate of seismogenic thickness implies that the entire crust
360 of the western foreland is seismogenic. Sloan and Jackson (2012) also identified two earthquakes
361 in the Arafura Sea which occurred in the seismogenic upper mantle. The deepest earthquake in
362 the New Guinea foreland (at 33 km) occurs within error of the Moho depth, however it is likely
363 the Moho depth in the foreland is depressed compared to where it was measured in the Arafura
364 Sea, due to the Australian plate bending as it underthrusts the mountains. Therefore it is more
365 likely this earthquake occurred within the lower crust than in the upper mantle. In the eastern
366 foreland basin between 141–146°E, the seismogenic thickness is resolvably thinner, and is 20–27 km.

367

368 It is more difficult to estimate the seismogenic thickness within the New Guinea Highlands
369 as we must differentiate between the earthquakes occurring within the seismogenic part of the
370 over-riding plate, those within the underthrusting Australian plate, and those linked with south-
371 dipping subduction at the New Guinea Trench. As the earthquake depths listed in the gCMT
372 or ISC-EHB Bulletin catalogues are less accurate than depths estimated using body-waveform
373 modelling (Engdahl et al., 2006), we have chosen to estimate the seismogenic thickness of the
374 Highlands using only the body-waveform modelled solutions from Abers and McCaffrey (1988). If
375 we consider all modelled events, T_s is between 46–48 km in the western Highlands (135–141°E) and
376 between 24–26 km in the eastern Highlands (141–146°E). The crustal thickness of the Highlands is
377 not well known, but is estimated to be ~ 45 km (Abers and McCaffrey, 1988; Abers and Lyon-Caen,
378 1990), so it is possible that the seismogenic thickness represents a single crustal layer. However,
379 the earthquakes are not distributed evenly through the crust in the western Highlands. Figure
380 5C shows that almost all earthquakes beneath the western Highlands occur at depths shallower
381 than 25 km. The deepest event, the reverse-faulting earthquake at 44 km and close to the range
382 front, may represent an earthquake in the underthrusting plate, whilst the shallower earthquakes
383 represent the seismogenic thickness of the upper plate. If this is the case, then the seismogenic
384 thickness of the over-riding material is similar between the western and eastern Highlands.

385 4.2 Thermal modelling

386 Changes in seismogenic thickness along-strike of the southern foreland basin correlate with changes
387 in lithosphere thickness (Figure 5A; Priestley et al., 2018). In this section we use thermal models
388 to examine whether the along-strike variation in seismogenic thickness could be the result of along-
389 strike variations in the thermal structure, due to the lithosphere thickness contrasts, or whether it
390 implies variations in composition. We have constructed simple steady-state geotherms for a range
391 of values of lithosphere thickness and radiogenic heating in the crust. We use a wide range of
392 values for lithosphere thickness to account for the broad horizontal resolution of the data (250–400
393 km). However, the east-west transition in lithosphere thickness is a major feature which stretches
394 southwards into Australia, so we are confident that the data reflect a true gradient in lithosphere

395 thickness along-strike of the basin.

396

397 In our thermal modelling, we have followed the methods of McKenzie et al. (2005), Copley
398 et al. (2009), and Craig et al. (2020). The one-dimensional diffusion equation has been discretised
399 and solved using a Crank-Nicholson (joint implicit-explicit) finite difference scheme (Press et al.,
400 1992). The upper surface of each geotherm was held at 0°C and the base of the lithosphere fixed
401 at the isentropic temperature for that depth, calculated using a mantle potential temperature of
402 1315°C. We follow the approach of Copley et al. (2009) and Craig et al. (2020) in approximating
403 the thermal boundary layer at the boundary between the lithosphere and the convecting mantle
404 as the isentropic temperature applied at that depth, which has minimal influence on the overlying
405 thermal structure. We use temperature-dependent values of thermal conductivity and heat capac-
406 ity (Hofmeister, 1999; McKenzie et al., 2005; Whittington et al., 2009), incorporating granodiorite
407 values for the crust (Miao et al., 2014) and olivine values for the mantle (McKenzie et al., 2005).
408 Steady-state geotherms are calculated by inputting an initial (arbitrary) thermal structure (in this
409 case a linear gradient from the surface to the base of the lithosphere), and allowing diffusion to
410 occur until the evolution through time is insignificant. The time taken depends on the lithosphere
411 thickness, which controls the thermal time constant of the lithosphere, and is < 1 Gyr. At each
412 time-step, we iterate multiple times, updating the temperature-dependent thermal parameters
413 with each iteration. Such a measure is necessary because our finite difference scheme is centred in
414 time, so the thermal parameters at the end of the time-step play a role in the computation (Press
415 et al., 1992). We therefore maintain self-consistent temperatures and thermal parameters at each
416 time-step.

417

418 Crustal thickness was held constant at 30 km (Jacobson et al., 1979; Clitheroe et al., 2000),
419 and radiogenic heating assumed to be constant throughout the crust, based upon recent results sug-
420 gesting that partial melting has a limited effect on the rate of radiogenic heating in the partitioned
421 melt and residue, due to the growth and/or retention of relatively high-Th accessory minerals in the
422 residue compensating for the removal of other heat-producing elements during partial melting and

423 melt migration (Yakymchuk and Brown, 2019, Weller et al., 2020). This assumption is consistent
424 with the lack of observed correlation between metamorphic grade and rate of radiogenic heating
425 in global compilations (Hasterok et al., 2018). Radiogenic heating in the mantle was assumed to
426 be zero, as model geotherms calculated with no mantle radiogenic heating correlate well with P-T
427 estimates from mantle xenoliths (e.g. Rudnick et al., 1998).

428
429 Figure 6A shows a collection of our calculated geotherms for which lithosphere thickness has
430 been varied but crustal thickness and crustal radiogenic heating have been held fixed (at 30 km and
431 $0.50 \mu\text{W}/\text{m}^3$ respectively), showing that increases in lithosphere thickness deepen the isotherms
432 throughout the lithosphere. In order to analyse the possible range in thermal structures in the
433 foreland, we have also performed calculations in which the crustal radiogenic heating has been
434 varied.

435
436 We first examine whether our observed earthquake distribution is consistent with the seismo-
437 genic thickness tracking the 600°C isotherm. This temperature has previously been suggested at
438 the upper limit of seismogenic behaviour in anhydrous rocks (of both crust and mantle litholo-
439 gies), based upon the comparison of earthquake depths and thermal models (Kohlstedt et al., 1995;
440 Mackwell et al., 1998; Lund et al., 2004; McKenzie et al., 2005; Jackson et al., 2008; Priestley et al.,
441 2008; Jackson et al., 2021). We investigate this case first because the New Guinea forelands are
442 comprised at least partially of Proterozoic high-grade metamorphic lithologies of the Australian
443 Shield (Plumb, 1979; Hill and Hall, 2003), and thus the crust may be anhydrous. We extracted
444 the depth to the 600°C isotherm from each calculated geotherm. These results are shown in Fig-
445 ure 6B, where the depth to the 600°C isotherm is plotted as a function of lithosphere thickness
446 and radiogenic heating. We then compared these depths to the observed seismogenic thickness of
447 the western and eastern foreland basin, to investigate whether the depth to the 600°C isotherm
448 represents the maximum possible seismogenic thickness. We chose to analyse the western and east-
449 ern halves of the basin separately given the differences in seismogenic and lithosphere thickness.
450 The blue and pink shaded regions show the parameter space over which the depth to the 600°C

451 isotherm is greater than or equal to the observed seismogenic thickness in the western and eastern
452 foreland basin respectively, and also where the lithosphere thickness used in our models matches
453 the observed thickness for each side of the basin (Priestley et al., 2018).

454

455 These results show that the modelled isotherm depth matches the observed seismogenic and
456 lithosphere thicknesses in both halves of the foreland basin. This means that the depth to the
457 600°C isotherm can vary laterally by the amount seen in the earthquake depths due to lateral
458 variations in the lithosphere thickness alone, without invoking changes in the composition of the
459 crust. We also note that radiogenic heating in the crust is required to be $\leq 1.5 \mu\text{W}/\text{m}^3$, which
460 is on the lower end of the range of values observed for crustal rocks (Hasterok et al., 2018) but
461 consistent with estimates of the overall heat budget of the continental crust (e.g. Rudnick et al.,
462 1998; Rudnick and Nyblade, 1999; Jaupart et al., 2015).

463

464 We have also considered the possibility that the foreland basin comprises hydrous crustal
465 material, which would be expected to supported earthquakes only up to temperatures of 350°C
466 (Chen and Molnar, 1983; Priestley et al., 2008). Hydrous continental crust might be expected in
467 the eastern foreland basin, on the east side of the Tasman Line, where the geology is comprised
468 of accreted Paleozoic terranes, instead of the older and thicker Australian craton observed in the
469 west (Crawford et al., 2003; Glen, 2005). This region east of the Tasman Line may not have been
470 subjected to the partial melting needed to generate anhydrous material. However, our modelling
471 shows that for the depth to the 350°C isotherm to be consistent with the observed seismogenic
472 thicknesses across the foreland basin, radiogenic heating in the crust would need to be < 0.25
473 $\mu\text{W}/\text{m}^3$, which is improbably low (see supplemental Figure S24, which is the equivalent of Figure
474 6B, but for the 350°C isotherm). Thus the seismogenic mid-crust of eastern foreland is unlikely
475 to be hydrous, despite the presence of overthrust Tasman Orogen units at the surface. These
476 results support our suggestion that the observed lateral variation in seismogenic thickness across
477 the foreland is primarily caused by the change in lithosphere thickness, and not a change in crustal
478 composition. The implications of these results are discussed further in Section 6.1.

4.3 Flexure and elastic thickness

Having investigated the seismogenic thickness and thermal structure of the southern foreland basin, we have also studied its elastic thickness. Elastic thickness is a useful proxy for the strength of the lithosphere as it bends in response to loading, and can be calculated using the wavelength over which this bending occurs, as observed using gravity anomalies. By studying both seismogenic thickness (T_s) and elastic thickness (T_e) of the foreland basin, we aim to contribute to the debate surrounding the rheology of continental lithosphere (e.g. McKenzie and Fairhead, 1997; Maggi et al., 2000b; Burov and Watts, 2006; Jackson et al., 2008).

Long-wavelength negative free-air gravity anomalies in the southern foreland basin suggest that the underthrusting Australian Plate is bending as a result of loading from the New Guinea Highlands (Figure 7A). These gravity anomalies can be used to estimate the effective elastic thickness of the foreland, which we have calculated using the method of McKenzie and Fairhead (1997), which is summarised here. Using the GOCE and EIGEN-6C datasets (Drinkwater et al., 2007; Förste et al., 2014), the two-dimensional gravity field was stacked into profiles perpendicular to the strike of the range-front. The observed gravity profiles were then compared to synthetic calculations. We invert for the best-fitting value of T_e , while allowing the magnitude and location of the vertical load and bending moment to vary, and also solving for a linear ramp that reproduces any long-wavelength signals in the data that are unrelated to flexure. The elastic thickness estimate obtained using this method is a measure of the effective elastic thickness of the bending layer within the lithosphere, but does not determine the depth to the top or bottom of this layer.

We modelled the west and east sides of the foreland basin separately, as well as calculating elastic thickness across the whole basin. We find the GOCE gravity anomalies between 135.5–141°E can be fit by a plate with an elastic thickness of 5 km, and between 141–143.5°E by an elastic thickness of 6 km (Figure 7D). Across the whole foreland basin (135.5–143.5°E), T_e is 5 km. Using the EIGEN-6C dataset, T_e is 5 km between 135.5–141°E, 11 km between 141–143.5°E, and T_e is 6 km across the whole basin. For most of these estimates, the misfit between the modelled

507 and observed gravity anomalies at large T_e values is only slightly greater than the minimum misfit,
508 producing a broad minimum, as can be seen for the eastern foreland basin on Figure 7D. This
509 effect is well known, and is caused by trade-offs between T_e , the bending moment, and the location
510 where the vertical load and bending moment are applied (often referred to as the plate break;
511 Jackson et al., 2008). When a broad minimum is observed, the upper bound is unconstrained and
512 so our results provide only a lower bound on elastic thickness. Our results do not allow us to
513 robustly use the gravity data to investigate whether there are lateral variations in T_e along-strike
514 of the mountains, so we propose that elastic thickness across the whole foreland basin is ≥ 5 km.

515

516 These results contrast with previous studies of the foreland basin, which found the effective
517 elastic thickness of the underthrusting Australian Plate to be up to 95 km and to vary significantly
518 along-strike (Abers and Lyon-Caen, 1990; Haddad and Watts, 1999). However these studies held
519 the plate break at a fixed position, which often leads to overestimates of T_e (Jackson et al., 2008).
520 The geographical position of the plate break is unknown, thus we prefer to allow the location of
521 the plate break to vary when calculating the misfit. The previous studies also studied single line
522 profiles whereas we chose to stack profiles along-strike of the range, which can lead to more stable
523 results (McKenzie and Fairhead, 1997; Jackson et al., 2008).

524

525 Although some of our estimates are lower bounds on the elastic thickness, some are well-
526 constrained (e.g. the green curve on Figure 7D). An elastic thickness of < 20 km is unexpected for
527 a foreland basin setting in which we have observed earthquakes at mid- and lower-crustal depths: in
528 both the western and eastern parts of the New Guinea foreland basin, the effective elastic thickness
529 we have estimated is significantly smaller than the seismogenic thickness inferred from earthquake
530 depths. Estimates of the elastic thickness from other geologically-similar regions have been found
531 to be greater, such as 17–25 km on the eastern foreland of the Andes and in northern India
532 (McKenzie et al., 2014; McKenzie et al., 2015), and Lamb et al. (2020) have suggested a global
533 trend in which the elastic thickness is 25–50% of the lithosphere thickness. However, our result is
534 similar to the work of Mitra et al. (2018), who studied the Shillong Plateau, a fault-bounded uplift

535 in the foreland basin in the Eastern Himalayas. They determined that the elastic thickness of the
536 Bengal Basin, to the south of the Shillong Plateau, is 5–20 km, which is considerably less than
537 the seismogenic thickness inferred from earthquake depths (40–45 km; Kumar et al., 2015). The
538 unusually low elastic thickness estimates from New Guinea and Shillong may therefore relate to
539 either (1) blanketing by large thicknesses of sediment, meaning that large proportions of the cool
540 and shallow crust are occupied by thick piles of (presumably weak) sediments that don't contribute
541 to the elastic strength, or (2) the geological position of both the Shillong Plateau and New Guinea
542 on the continental margin of an underthrusting plate, which may indicate an inherent weakness in
543 these margins. In either case, where constraints can be placed on the upper bound, our estimate
544 of the elastic thickness is less than our observed seismogenic thickness.

545 **4.4 Summary of New Guinea Highlands and forelands**

546 Our results show that there is along-strike variation in seismogenic thickness in the southern
547 foreland basin of the New Guinea Highlands. Thermal modelling suggests that this is likely to
548 be due to lateral variations in lithosphere thickness, rather than crustal composition, such that
549 thicker lithosphere in the west correlates with greater seismogenic thickness. Modelling the gravity
550 anomalies observed in the foreland basin has shown the elastic thickness in both the western and
551 eastern halves of the basin to be small (≥ 5 km, and < 20 km where the upper bound is constrained),
552 and that $T_e < T_s$ across the whole basin. The implications of these results will be discussed in
553 Section 6.

5 Normal faulting in the Bird's Head Block

Having studied the present-day tectonics of the New Guinea Highlands and foreland basin, we now turn our attention to the Bird's Head Block of western New Guinea, in order to further investigate the rheology and evolution of the deformation belt. The Bird's Head Block incorporates the Bird's Head, Neck, and Cenderawasih Bay (Stevens et al., 2002; Baldwin et al., 2012). We have used earthquake source parameter estimates, seismic reflection profiles, published geodetic results, and geomorphological observations to examine the characteristics of earthquakes in this region, and to study how the regional tectonics may have changed through time.

5.1 Normal faulting

A cluster of normal-faulting earthquakes within the Bird's Neck and the west side of Cenderawasih Bay indicate that the area is experiencing active extension (Figures 3 and 4). Body-waveform modelling and depth-phase analysis we conducted on 5 normal earthquakes in this region have shown that these events are characterised by approximately N-S striking nodal planes and shallow depths of 10 km or less (Table 1 and 2; Figure 8). These results emphasise the importance of body-waveform modelling and depth-phase analysis to estimate accurate source depths: of the 5 earthquakes we modelled, the ISC-EHB Bulletin lists their depths 25 km deeper on average (Weston et al., 2018; International Seismological Centre, 2020).

Using the source depths of our modelled earthquakes, we have estimated the seismogenic thickness (T_s) of the Bird's Neck to be approximately 15 km. This estimate of T_s from seismological observations is consistent with the local fault-controlled topography, as the maximum widths of extensional fault-bounded basins have been found to relate to the depth extent of the faults (Jackson and White, 1989; Scholz and Contreras, 1998). Within the Lengguru Fold-Thrust Belt in the Bird's Neck, high-resolution SRTM 30 m topography data (Farr et al., 2007) reveal several fault-bounded basins with a maximum width of 18 km (Figure 9). The basin width–seismogenic thickness scaling relationship of Copley and Woodcock (2016) yields an estimate of T_s between

580 12-18 km for that maximum basin width, which is consistent with the seismological estimate. This
581 result also shows that the Bird's Neck has a lower seismogenic thickness than the foreland basin
582 in central New Guinea. Many studies suggest that the Bird's Head Block represents the northern
583 margin of the Australian continent (e.g. Hamilton, 1979; Dow and Sukamto, 1984; Hill and Hall,
584 2003). The low seismogenic thickness might result from the Bird's Neck representing a thinned
585 continental margin, or because the Paleozoic metasediments which comprise the basement geology
586 are likely to be weaker than the Precambrian craton which underlies the western foreland basin in
587 central New Guinea (Visser and Hermes, 1962; Pieters et al., 1983; Bailly et al., 2009).

588

589 To further study the nature of extension in western New Guinea, we have estimated geodetic
590 strain rates across the region using the triangulation method of Bourne et al. (1998) and the GPS
591 data of Stevens et al. (2002). This method was selected because the GPS network across New
592 Guinea is sparse, and so it is more suitable to calculate strain rates within discrete triangles than
593 to calculate strain rate as a continuous field. The region of interest was split into triangles with a
594 GPS site located at each vertex. The strain rate within each triangle was calculated via a linear,
595 piece-wise continuous interpolation across the triangular region, using the three GPS velocities.
596 The strain rate within each triangle is equal to the average strain rate obtained from a continuous
597 strain rate field over the same region, and is independent of the choice of geodetic reference frame.
598 Our geodetic analysis is shown in Figure 8, alongside a summary of normal faulting in western
599 New Guinea. The GPS data show that the Bird's Head Block is moving rapidly with respect
600 to the Australian Plate. The strain rate analysis matches our observations of seismicity across
601 the region: extension occurs approximately E-W across Cenderawasih Bay, the Bird's Neck, and
602 further south towards the Aru Trough. Rapid left-lateral shear strain is also observed across the
603 north coast of the island, coincident with the location of the Sorong and Yapen Fault Zones. We
604 find that the orientation of extensional strain on the west side of Cenderawasih Bay is consistent
605 with the calculated slip vectors for normal earthquakes in the region, such that the extension
606 is most likely accommodated by slip on these shallow normal faults. We note that the smaller
607 component of \sim N-S compression in the region may be related to locking on the megathrust to

608 the north (but that this source of deformation would be unable to reproduce the observed \sim E-W
609 extension). Because the errors on the GPS velocity estimates (2–3 mm/yr) are small compared
610 with the velocity differences across the triangles (up to 125 mm/yr), these results are robust.

611 **5.2 Tectonic changes through time**

612 Whilst the Bird’s Neck and Cenderawasih Bay are currently experiencing E-W extension, topo-
613 graphic structures imply that the region has undergone several stages of tectonic deformation
614 during the Neogene. The Lengguru Fold-Thrust Belt (LFTB) within the Bird’s Neck comprises
615 anticlinal folds striking approximately NW-SE, formed of Mesozoic shelf sediments from the Aus-
616 tralian passive margin above Paleozoic metasedimentary basement (Figure 9; Visser and Hermes,
617 1962; Dow and Sukamto, 1984; Moffat et al., 1991; Bailly et al., 2009). Analysis of offshore seismic
618 lines and petrological analysis of metamorphic rocks from Wandamen Bay has constrained the
619 timing of formation of the LFTB to between 11–2 Ma (Bailly et al., 2009; de Sigoyer et al., 2011;
620 François et al., 2016; White et al., 2019).

621
622 Using the SRTM 30 m DEM, we have identified two groups of normal faults in the Bird’s
623 Neck (Figure 9). One set of faults in the southwest of the Bird’s Neck strike NE-SW and cut
624 across the LFTB at a high angle (Set 1). Anticlines which are cut by these faults show vertical
625 offsets in the topography of 150–700 m. There appear to be no recent earthquakes associated with
626 these faults within the fold-thrust belt. However, the clear geomorphological expression of these
627 faults suggests that it is possible the faults are active, and the lack of seismicity could be due
628 to the combination of low strain rates and the length of the instrumental earthquake catalogue.
629 A second set of normal faults near the Wandamen Peninsula strike approximately N-S and may
630 be associated with the recent normal-faulting earthquakes along the west side of Cenderawasih
631 Bay (Set 2). These normal faults run parallel to the major anticline which forms the Wandamen
632 Peninsula, so these faults may represent reactivated thrust faults from the formation of the LFTB,
633 or from the emplacement of the Weyland Overthrust: a block of metamorphosed sediments and
634 ophiolite slices which was thrust \sim 25 km southwest in the late Miocene (Dow and Sukamto, 1984;

635 Baily et al., 2009; François et al., 2016). The change in fault orientation between Set 1 and Set
636 2 may represent a change in the direction of strain being experienced within the Bird’s Neck in
637 either space or time. It has also been suggested that movement of the Bird’s Head Block relative
638 to Australia may be at least partially accommodated by vertical axis rotations of large crustal
639 blocks (Stevens et al., 2002). This theory might explain the discrepancy between the orientation
640 of the geomorphologically-clearer faults in Set 1 (striking NE-SW) and the focal mechanisms of
641 the recent normal earthquakes (striking N-S and with slip vectors aligned with the extensional
642 principal axes calculated from the GPS data).

643

644 To further investigate the timing of tectonic changes in the region through time, we have
645 analysed a seismic reflection profile in the north of Cenderawasih Bay (line location indicated in
646 Figure 8). This seismic line was originally presented by Priastomo (2012), and we have updated
647 the ages of the main horizons using the results of Babault et al. (2018). In the northwestern part
648 of the seismic reflection profile, the data show a fold-and-thrust system which has deformed the
649 Oligocene-Miocene sedimentary sequence (Figure 10). This period of shortening appears to have
650 ended by 3.6 Ma, as shown by the undeformed covering of sediments of this age (blue dotted
651 horizon in Figure 10 above the folds; Priastomo, 2012). The sedimentary sequence has then been
652 displaced by extensional faults that appear to be active at present. Fault A (indicated in Figure
653 10) has a prominent bathymetric expression, with ~ 1.5 km relief (equivalent to ~ 2 seconds two-
654 way travel time) and with apparently larger displacements in the underlying sedimentary units.
655 Fault B shows growth in the uppermost parts of the stratigraphy, including a horizon dated at
656 ~ 63 –480 ka (orange dotted line; Babault et al., 2018). Sedimentary growth is seen only in the
657 uppermost units of the Pliocene-Recent sequence. These observations indicate a tectonic change
658 from compression to extension occurred in this region at some time after 3.6 Ma.

659

660 In the southeastern part of the seismic reflection profile, the seismic horizons are affected by
661 NE-SW trending folds and thrust faults, which are rooted in a detachment within the Pliocene-
662 Quaternary sedimentary column (Decker et al., 2009; Priastomo, 2012; Babault et al., 2018). This

663 region has been named the Cenderawasih Fold-and-Thrust Belt (Priastomo, 2012) or Waipoga Fold-
664 and-Thrust Belt (WFTB; Babault et al., 2018). Rather than representing tectonic deformation,
665 the WFTB is interpreted as a toe-thrust system resulting from gravitational instability in the
666 external part of the sedimentary prism, which is up to 12 km thick and where sedimentation rates
667 could have reached very high values during the last 3 My (Babault et al., 2018). The WFTB
668 formed after the LFTB in the Bird’s Neck, and the base of the syn-tectonic sediments is dated
669 at $\sim 63\text{--}480$ ka (Babault et al., 2018). Hence, deformation in the WFTB is probably no older
670 than late Pleistocene. The seismic reflection profile shows that compressive folding and thrusting
671 in the upper sedimentary sequence in this area does not affect the lower sedimentary sequence
672 and basement. This is consistent with the interpretation of the shortening being due to localised
673 gravitational instability within the sedimentary pile, rather than representing crustal-scale tectonic
674 deformation. We discuss below the implications of the changing tectonic configuration through
675 time in the region of the Bird’s Neck and Cenderawasih Bay.

6 Interpretations and discussion

6.1 Reconciling observations of earthquake depths, lithosphere thickness, and elevation

Body-waveform modelling and depth-phase analysis of earthquakes in the New Guinea foreland basin has shown that the seismogenic thickness of the foreland varies along-strike, being greater in the west than the east. This variation in seismogenic thickness correlates with an along-strike variation in lithosphere thickness, derived from surface wave tomography, such that thicker lithosphere is observed in the areas of greater seismogenic thickness (Figure 5; Priestley et al., 2018). Using simple thermal modelling techniques, we have shown that the variation in seismogenic thickness in the foreland basin can be attributed solely to the changing lithosphere thickness, without having to invoke any variation in other parameters such as crustal composition. The 600°C isotherm, which is commonly thought to represent the depth extent of earthquakes in anhydrous continental crust (e.g. Jackson et al., 2021), is located deeper in thicker lithosphere and thus allows earthquakes to occur at greater depths.

It is surprising that the seismogenic thickness in the eastern part of the foreland appears to be governed by the 600°C isotherm, given that, in contrast to the high-grade and anhydrous metamorphic rocks and thick lithosphere that usually characterise where earthquakes occur at such high temperatures (Mackwell et al., 1998; McKenzie et al., 2005; Jackson et al., 2021), the region has relatively thin lithosphere and is believed to be formed of accreted island arc, back arc, and forearc terranes of the Tasman Orogen (Crawford et al., 2003; Hill and Hall, 2003; Glen, 2005). Within these accreted terranes, it might be expected that earthquakes in the eastern foreland would be limited to material at temperatures $< 350^{\circ}\text{C}$, as is observed in regions of hydrous crust which have not undergone partial melting (Priestley et al., 2008). However, as described in Section 4.2, for reasonable values of radiogenic heating, the observed seismogenic thickness in the eastern part of the foreland is much greater than the depth to the 350°C isotherm calculated from

our thermal modelling. We suggest that the observed seismogenic thickness may be due to two factors. First, the Tasman Orogen was formed in the Paleozoic above a west-dipping subduction zone, and oceanic terranes were progressively thrust over and onto the Precambrian rocks of the Australian continental interior (Coney et al., 1990; Veevers, 2000; Crawford et al., 2003; Glen, 2005). It is therefore possible that the strong, anhydrous, high-grade metamorphic rocks of the Australian craton form the mid-to-lower crust in the eastern New Guinea foreland, which have been overthrust by the Tasman Orogen. This suggestion is supported by Aitchison et al. (1992), who analysed zircons from the basement of the New England Orogeny in eastern Australia and concluded that terranes of the Tasman Orogen have been “thrust a considerable distance over the continental freeboard of eastern Australia”. Second, east-west rifting along the northeastern margin of the Australian continent in the late Cretaceous-early Eocene, which formed the Coral Sea (Figure 1B), is likely to have thinned the lithosphere along this margin (Weissel and Watts, 1979; Davies et al., 1997; Gaina et al., 1999). These two factors combined could result in anhydrous and seismogenic mid-to-lower crust in a region of thin lithosphere, with an absence of high-grade anhydrous rocks at the surface. This situation would allow for earthquake depths across the whole foreland basin to be limited by the depth to the 600°C isotherm, the location of which is controlled by lithosphere thickness and the resulting temperature structure.

719

An additional observation to consider is the elevation of the New Guinea Highlands. There is a long-established concept that the maximum height that can be achieved by a mountain range depends on the strength of the bounding forelands (Dalmayrac and Molnar, 1981; England and Houseman, 1988; Molnar and Lyon-Caen, 1988). Therefore we might expect the western Highlands to have a significantly higher elevation than the east, due to the thicker, cooler, stronger foreland. However, in New Guinea, although the seismogenic and lithosphere thickness vary and correlate along-strike, the elevation of high, low-relief plateau-like regions of the mountain range are very similar in the east and west (Figure 5B). This consistency might be explained if the mountains have not yet reached their limiting elevation (the maximum elevation which can be supported by the forelands). However, the Highlands show little evidence of active crustal thickening (Figure

730 4); instead the thrust faulting has stepped southwards onto the range front (Figure 3; Visser and
731 Hermes, 1962; Hamilton, 1979; McCaffrey and Abers, 1988). This observation suggests that the
732 New Guinea Highlands have reached their current limiting elevation. The low-relief interior of the
733 ranges implies that their elevation is not controlled by erosion, in which case they would be char-
734 acterised by actively-incising drainage. The lack of correlation between elevation and seismogenic
735 thickness therefore warrants an explanation.

736

737 To examine how the mountain range elevation might be related to the thickness and thermal
738 structure of the underthrusting lithosphere, we have calculated the forces acting between the New
739 Guinea Highlands and forelands. Mountains have a higher gravitational potential energy than
740 their forelands, due to the work done against gravity when thickening the crust. The horizontal
741 force per unit length exerted between a mountain range and its foreland, caused by this contrast
742 in potential energy, can be calculated from the lateral differences in density structure between the
743 two regions (Artyushkov, 1973; Dalmayrac and Molnar, 1981).

744

745 We consider the New Guinea Highlands and forelands as isostatically-balanced columns which
746 have a vertical density structure controlled by the temperature, composition, and thickness of the
747 crust and lithospheric mantle. Lateral differences between these density structures will generate
748 horizontal gradients in vertical normal stress. By integrating the vertical normal stress from the
749 surface to the depth of isostatic compensation, we can obtain the horizontal force per unit length
750 acting between the mountains and the forelands (Artyushkov, 1973; Dalmayrac and Molnar, 1981).
751 We assume that the New Guinea Highlands have reached the maximum elevation which can be
752 supported by the forelands, because the mountains are dominated by strike-slip faulting and the
753 reverse faulting has migrated into the foreland basin (Figure 3). This assumption allows us to use
754 the potential energy contrasts to explicitly estimate the horizontal force exerted on the forelands
755 (Dalmayrac and Molnar, 1981).

756

757 We performed separate calculations for the western and eastern regions, separated at 141°E,

758 due to the observed along-strike variation in lithosphere thickness. Following the methods of Cop-
759 ley and Woodcock (2016) and Wimpenny et al. (2018), which are built upon Lamb (2006), we have
760 varied the model parameters throughout the range geological plausible values in order to estimate
761 a range of possible force magnitudes (Table 3), as described here. To calculate the vertical density
762 structures, we take the crustal thickness in the forelands to be 30–35 km, based on receiver function
763 studies in the Arafura Sea (Jacobson et al., 1979; Clitheroe et al., 2000), and 40–60 km in the
764 mountains, where the value is less constrained (Abers and McCaffrey, 1988; Abers and Roecker,
765 1991). Lithosphere thickness is taken from the measurements of Priestley et al. (2018). Geotherms
766 in both the mountains and forelands were assumed to be in steady state, and consist of 2 linear
767 sections between the surface and the Moho, and the Moho and the base of the lithosphere (which
768 is enforced to be at the isentropic temperature, given a mantle potential temperature of 1315°C).
769 Estimates of Moho temperature in the forelands were derived using the geotherms calculated in
770 Section 4.2 and the estimates of crustal thickness. Moho temperatures in the mountains were
771 varied over a wide range to account for uncertainties in thermal structure and crustal thickness
772 estimates. The average density (at 0°C) of the crust in the forelands and mountains were taken
773 to be 2800 kg/m³ (Turcotte and Schubert, 2002). We used a thermal expansion coefficient of 3 x
774 10⁻⁵ K⁻¹ to model the density changes in the crust caused by temperature (Turcotte and Schubert,
775 2002). The density of the lithospheric mantle is taken to be 60 kg/m³ less than the density of the
776 asthenosphere at the same P-T conditions. We used the results of Bouhifd et al. (1996) to model
777 the thermal expansion of the lithospheric mantle.

778

779 By varying all input parameters, we estimate that the horizontal force exerted between the
780 western Highlands and foreland is $2.5\text{--}5 \times 10^{12}$ N per metre along-strike of the range, and $2\text{--}4.5 \times 10^{12}$
781 N/m between the eastern Highlands and forelands (Figure 11A), therefore showing little along-
782 strike variation. This situation is to be expected, because generally the horizontal force exerted
783 between a mountain range and its lowlands scales with elevation. For example, the forces across the
784 New Guinea Highlands are larger than those calculated for the mountains of Albania (1.2×10^{12}
785 N/m; Copley et al., 2009), where mean elevation is only ~ 1 km compared to 2–3 km in New

786 Guinea. However in the Andes, where elevation is 4–5 km, the horizontal force between the Andes
787 and South American lowlands is $4\text{--}8 \times 10^{12}$ N/m (Wimpenny et al., 2018), which is larger than the
788 forces seen in New Guinea.

789

790 To reconcile our observations of seismogenic thickness, thermal structure, and elevation, we
791 propose that the current elevation of the Highlands has been set by the thin passive margin ma-
792 terial on the northern margin of the Australian plate which was involved in the initial stages of
793 the orogeny. Mountain building began around 15 Ma, with the northwards underthrusting of thin
794 continental lithosphere from the northern passive margin of Australia. Triassic rifting along this
795 northern margin had truncated the Tasman Orogen in eastern New Guinea, and formed a $\sim 1,000$
796 km wide shelf underlain by thinned continental crust (Pigram and Panggabean, 1984; Cloos et al.,
797 2005). Thus the initial stages of mountain building presumably involved the underthrusting of
798 lithosphere that would have been thinner, hotter, and weaker than that now underthrusting the
799 western part of the range (Figure 12). Only recently has thicker continental crust and lithosphere
800 from the Australian Plate been underthrusting the mountains (beginning 10–8 Ma; Cloos et al.,
801 2005), with cold, strong cratonic material in the west but the continued underthrusting of thinner,
802 weaker lithosphere in the east due to the along-strike variability in the lithosphere structure. It is
803 likely that crustal thickness and elevation in the Highlands have not yet readjusted to the arrival
804 of stronger material in the west and have not reached the maximum elevation as can be supported
805 by the stronger forelands. Over time, we expect the elevation of the western Highlands to grow
806 in response to the increased strength of the cold cratonic foreland crust (Figure 12). This concept
807 highlights the possible effects of lateral variations in lithosphere strength on the evolution of to-
808 pography during the initial stages of mountain building.

809

810 The New Guinea Highlands have lower elevation than long-lived mountain ranges like the An-
811 des (~ 4 km) and the Tibetan Plateau (4–5 km). Despite the underthrusting material increasing
812 in strength over time, the current New Guinea foreland also has a lower seismogenic thickness and
813 elastic thickness than northern India and the Andean foreland (e.g. Assumpção and Suárez, 1988;

814 McKenzie and Fairhead, 1997; Maggi et al., 2000b; Pérez-Gussinyé et al., 2007; McKenzie et al.,
815 2014). These comparisons emphasize the importance of spatial variability in the underthrusting
816 plate in controlling the evolution of the bounding mountain ranges, for while northern India and
817 the Andean foreland represent strong continental interiors, New Guinea represents a weak conti-
818 nental margin which supports lower elevation mountains. However, as more Australian material is
819 underthrust and the forelands gradually come to be composed of strong continental interior (e.g.
820 the region in the central Arafura Sea which supports upper mantle earthquakes at 61 km depth;
821 Sloan and Jackson, 2012), the New Guinea Highlands may eventually reach elevations similar to
822 the Andes and Tibet.

823 **6.2 Foreland deformation and fault strength**

824 There are two lines of evidence which suggest that the western and eastern New Guinea foreland
825 are deforming differently. First, there are broad-scale differences in the topography of the foreland
826 basin. In the east lies the Darai Uplift, which is situated south of the range front (Figure 1B).
827 Also referred to as the Darai Plateau or Darai Anticline, this structure is 150 km long and reaches
828 a maximum elevation of ~ 1 km above the surrounding foreland. The Darai Uplift is a single
829 basement-cored anticline which is thought to represent shortening on a major basement-involved
830 thrust fault, which itself may be a reactivated extensional fault generated by Mesozoic passive
831 margin rifting (Hobson, 1986; Hill, 1991; Buchanan and Warburton, 1996). In contrast, the west-
832 ern foreland basin shows no large-scale structures comparable to the Darai Uplift and appears to
833 be mostly “unbroken”. The overlying fold-thrust belt appears to be relatively thin-skinned, and
834 consists primarily of en echelon folding with kilometre-scale subsidiary thrust faulting (Granath
835 et al., 1991; Cloos et al., 2005).

836

837 The second line of evidence concerns active faulting in the foreland basin. Our earthquake
838 modelling has revealed high-angle reverse faulting earthquakes with nodal planes striking paral-
839 lel to the range front (Figure 3). In the western foreland basin between $135\text{--}141.5^\circ$, it does not
840 appear that the earthquakes are breaking through the entire seismogenic foreland. The isolated

841 M_w 5.2 earthquake at 33 km depth in the western foreland is separated from the shallower events
842 by an apparently aseismic middle crust, and the deep event is not large enough to have ruptured
843 the entire seismogenic layer. In contrast, the eastern foreland basin between 141.5-145° contains
844 earthquakes for which the depths span the whole of the seismogenic layer. In conjunction with
845 the presence of the Darai Uplift in the eastern foreland basin, these observations imply that the
846 force being exerted between the mountain range and the Australian foreland is large enough to
847 break the entire thickness of the crust in the eastern foreland basin, but not in the west. This
848 pattern is consistent with our logic described above that the western foreland is stronger than the
849 east because of the thicker lithosphere leading to cooler temperatures in the crust and a thicker
850 seismogenic layer.

851

852 For reverse faulting to occur throughout the crust in the eastern foreland, the horizontal com-
853 pressive forces acting between the Highlands and forelands must be large enough to exceed the
854 static frictional strength of the faults. In this setting, we are therefore able to estimate the rheology
855 of these faults (Copley et al., 2011). In contrast, where the foreland is not deforming, although
856 the type of analysis shown in Figure 11A can estimate the force transmitted through the foreland,
857 it is only possible to place a lower bound on the fault strength. In order to estimate the frictional
858 properties of the faults breaking the eastern New Guinea foreland, we have followed the method of
859 Wimpenny et al. (2018) by constructing one-dimensional yield stress profiles which represent the
860 stress state with depth. By integrating the yield stress over depth, we can estimate the force per
861 unit length which the foreland lithosphere can support ($F = \int \Delta\sigma_{xx} dz$; where F is force per unit
862 length, $\Delta\sigma_{xx}$ is horizontal differential stress, and z is depth). We have undertaken this process for
863 a range of different rheological parameters, as described below. By comparing the forces estimated
864 by these calculations with our estimate of the horizontal force exerted between the mountains and
865 lowlands as described above, we can place an upper bound on the frictional strength of faults in
866 the eastern New Guinea forelands.

867

868 We performed a parameter sweep through the range of variables which control the shape of the

869 yield stress envelope with depth, as listed in Table 3 (sediment thickness, seismogenic thickness,
870 fault dip, neutral fibre depth, elastic core thickness, sediment thickness, and effective coefficient of
871 friction). As with the force calculations above, this process was undertaken due to the uncertainty
872 in the values of some variables. We have also considered the creep strength of the lithospheric
873 mantle in our calculations, as follows. Earthquake source modelling has shown that there is lit-
874 tle evidence for deep earthquakes occurring within the foreland mantle lithosphere (Figure 5).
875 This observation, and the comparison between the seismogenic and elastic thickness estimates de-
876 scribed above, suggest that the horizontal forces are mostly supported by frictional stresses within
877 the seismogenic crust. We assume that at temperatures above 600°C, the mantle deforms mostly
878 by ductile creep. We use a dry olivine dislocation creep law (Karato and Wu, 1993), which gives
879 an upper bound on the ductile strength of the lithospheric mantle and thus a lower bound on the
880 frictional strength of crustal faults. At temperatures $< 750^\circ\text{C}$, it has been suggested that the upper
881 mantle may deform plastically via Peierl’s Creep (Mei et al., 2010; England and Molnar, 2015),
882 which gives a lower estimate of ductile mantle strength than when dislocation creep is assumed.
883 However, we have also performed calculations in which the lithospheric mantle has zero strength,
884 which gives an absolute upper bound on the frictional strength of crustal faults.

885

886 Our results show that in order to break in response to the $2\text{--}4.5 \times 10^{12}$ N/m horizontal force
887 transmitted between the mountains and the foreland, the effective coefficient of friction for crustal
888 faults in the eastern New Guinea forelands must be < 0.28 , if we assume the lithospheric mantle
889 deforms by dislocation creep above 600°C (Figure 11B). These coefficients of friction are equivalent
890 to depth-averaged differential stresses of ≤ 104 MPa. The nominal most likely value for the effective
891 coefficient of friction is 0.125, equivalent to a depth-averaged differential stress of 46 MPa. If the
892 lithospheric mantle supports no stress whatsoever, the maximum effective coefficient of friction in
893 the forelands is 0.31 (corresponding to depth-averaged differential stresses of ≤ 115 MPa).

894

895 In the western foreland basin, we do not see evidence for basement-cored anticlines and the
896 earthquakes are not distributed throughout the crust (Figure 5). Thus the crust does not appear

897 to be breaking through on faults in the same way as in the eastern foreland basin. The western
898 foreland must therefore be strong enough to support the horizontal forces exerted between the
899 mountains and the lowlands, which we estimated to be $2.5\text{--}5 \times 10^{12}$ N/m along-strike. Therefore,
900 the strength of these faults in the western foreland cannot be estimated, and only a lower bound
901 placed upon this value (i.e. that we know they must be strong enough to not deform in response to
902 the applied forces). Using the same frictional analysis as for the eastern foreland, we can therefore
903 calculate the minimum coefficient of friction needed to support the observed horizontal forces. Our
904 analysis shows that the lower bound on the effective coefficient of friction in the western foreland is
905 between 0.01–0.14. It is likely that faults in the western and eastern foreland have similar strength,
906 but the greater seismogenic thickness of the western foreland allows it to support the horizontal
907 force (which is very similar across the east and west forelands) without breaking. Assuming fault
908 strength is similar across the foreland basin and that the mantle deforms via dislocation creep, we
909 can therefore constrain the effective coefficient of friction of faults in the New Guinea foreland to
910 be between 0.01–0.28.

911

912 Our results are consistent with similar studies of foreland regions, which found low estimates
913 of the effective coefficient of friction in the Variscan forelands (< 0.24 ; Copley and Woodcock,
914 2016), the Peruvian Andes (< 0.15 ; Wimpenny et al., 2018), and the northern Indian shield ($<$
915 0.3 ; Bollinger et al., 2004; Herman et al., 2010; Copley et al., 2011). While these geophysical
916 studies show consistent results, they are significantly lower than traditional laboratory estimates
917 of dry rock friction (0.6–0.8; Byerlee, 1978). This suggests that the foreland faults may be weak
918 because they are reactivated structures containing phyllosilicate-rich fault gouges (Imber et al.,
919 2008; Lockner et al., 2011; Remitti et al., 2015), or because they are subjected to elevated pore
920 fluid pressures (Sibson, 2004).

921 **6.3 Tectonic evolution of western New Guinea**

922 Having constrained the present-day rheology and force balance in the New Guinea Highlands and
923 their southern forelands, we now investigate the evolving force balance in western New Guinea. As

924 described above, analysis of normal-faulting earthquakes, GPS data, geomorphology, and seismic
925 reflection profiles has shown that the Bird's Neck and Cenderawasih Bay are presently undergoing
926 extension, but have been subjected to several stages of tectonic evolution throughout the Neogene
927 and Quaternary (Figure 8, Figure 9, and Figure 10). The Lengguru Fold-Thrust Belt (LFTB)
928 shows that the Bird's Neck has experienced significant crustal shortening, but has since been cut
929 by more recent extensional faults observed both onshore within the LFTB and Wandamen Penin-
930 sula, and offshore in Cenderawasih Bay. Structural and sedimentological analysis suggests that
931 the LFTB formed between 11–2 Ma (Bailly et al., 2009). This shortening may have been caused
932 by the Weyland Overthrust: a rifted continental sliver which was thrust ~ 25 km southwest over
933 the Bird's Neck in the late Miocene, due to localised subduction in Cenderawasih Bay (Dow and
934 Sukamto, 1984; Hill and Hall, 2003). de Sigoyer et al. (2011) and François et al. (2016) analysed
935 metamorphic assemblages from the Wandamen Peninsula and suggested that the rocks had been
936 buried to 45 km depth at 8 Ma, followed by rapid exhumation around 5 Ma. Further metamorphic
937 dating in the Wandamen Peninsula led White et al. (2019) to argue that formation of the LFTB
938 was even younger, occurring between 5–3 Ma. Dating of the undeformed sediment layers observed
939 in the western part of the seismic reflection profile, which blanket the fold-thrust belt, imply that
940 shortening had ceased by 3.6 Ma (Figure 10; Priastomo, 2012). Most studies agree, however, that
941 there was a shift to regional transtension approximately 2 Ma, which generated the cross-cutting
942 normal faults seen in Figure 9. This event was coeval with the generation of the Tarera-Aiduna
943 Fault, and the initiation and reactivation of normal faults within the Paniai-Lowlands Fault Zone
944 (Puntodewo et al., 1994; Stevens et al., 2002; Pubellier and Ego, 2002; Bock et al., 2003; Bailly
945 et al., 2009).

946

947 While this switch from tectonic compression to transtension in the early Pleistocene is gen-
948 erally accepted, it is uncertain what triggered this change in tectonic regime. Bailly et al. (2009)
949 have previously attributed the cessation of shortening within the Lengguru Fold-Thrust Belt to
950 slab rollback at the Seram Trench (Figure 1B) and increasing friction during the development
951 of the accretionary prism. They suggest that localised shortening within the LFTB, as a result

952 of Australia-Pacific convergence, was transferred to the Seram Trench and adjacent accretionary
953 prism after the formation of the Tarera-Aiduna Fault. However, this explanation does not explain
954 the presence of normal-faulting roughly orthogonal to the previous shortening direction, and so
955 other factors must also be involved. The other major tectonic change in the region at a similar
956 time is the evolution of the Banda Arc. Spakman and Hall (2010) proposed that the extreme
957 curvature of the Banda Arc has developed over the last ~ 15 My as the Banda oceanic slab rolled
958 back and the arc moved eastwards towards Australia and New Guinea. They suggest that the
959 arc's curvature increased over time due to the subduction of a Jurassic oceanic embayment on the
960 northwest margin of the Australian Plate, and the progressive folding of a single subducted slab
961 at depth. We therefore investigate whether increasing curvature in the Banda Arc through time
962 could have resulted in the change in tectonic style in western New Guinea around 2 Ma.

963

964 A summary of the tectonic evolution of western New Guinea is shown in Figure 13, based on
965 work by Pubellier and Ego (2002), Hill and Hall (2003), Bailly et al. (2009), Spakman and Hall
966 (2010) and François et al. (2016). The development of increasing curvature in the Banda Arc will
967 have increased the circumference of the Bird's Head Block, and thus also the magnitude of the plate
968 driving forces exerted upon the block by the Banda Arc. We will here test whether this increase
969 in force along the Banda Arc may have been responsible for the initiation of the Tarera-Aiduna
970 Fault, reactivating faults in the Paniai-Lowlands Fault Zone, and changing the tectonic regime in
971 the Bird's Neck and Cenderawasih Bay.

972

973 We have tested this hypothesis by performing simple force-balance calculations across the
974 Bird's Head Block. In these calculations, we have chosen to model the Bird's Head Block as a
975 rigid undeforming block, and to balance the forces acting upon it. This approach is motivated by
976 there being negligible internal deformation within the BHB revealed by earthquakes (Figure 4) or
977 GPS (Figure 8), and there being a series of long, rapidly slipping, fault zones on it's boundaries.
978 In this case, balancing forces on a rigid block is more appropriate than modelling the region as a
979 continuum (England and McKenzie, 1982). Because the topography strikes parallel to the fault

980 zones bounding the block, any gravitational potential energy contrasts across these boundaries
981 are included within the net forces on the boundaries that we investigate below. Additionally,
982 provided that any basal drag on the base of the Bird's Head Block is parallel to the direction of
983 motion on the subduction interface (i.e. that the mantle flow is controlled by the subducting slab),
984 then this component of the force balance is also captured in the net force exerted by the Banda arc.

985

986 The main forces exerted upon the Bird's Head Block are caused by the major fault zones
987 along its edges, namely the Banda Arc (subduction zone force) and the Sorong-Yapen Fault Zone
988 in the north (shear zone force; Figure 14A). By varying the forces exerted by these two major
989 fault zones, and assuming that the net force exerted upon the Bird's Head Block is zero, we can
990 resolve the forces to find the resultant force acting on the Bird's Neck and the eastern margin of
991 Cenderawasih Bay (Figure 14B). We can then compare this resultant force with the orientations
992 of the fault zones and the slip vectors of earthquakes, to determine whether there is a combination
993 of forces which may have been consistent with generating or reactivating the faults in this area,
994 and creating the pattern of strike-slip and normal faulting observed today.

995

996 To calculate the possible net forces exerted on each boundary of the Bird's Head Block, we
997 multiply the length of each fault zone along the block boundaries with a range of plausible values
998 for the net force per unit length transmitted across the block boundaries. We use the present-
999 day geometries of the fault zones to estimate the lengths, and assume that the fault zones have
1000 undergone insignificant geometric change over the past 2 My. The main uncertainty in these cal-
1001 culations is the force per unit length exerted across the block boundaries, and so we have varied
1002 this value over a wide range. To reflect the global uncertainty in the force balance in subduction
1003 zones (Forsyth and Uyeda, 1975; Conrad and Hager, 1999; Billen and Gurnis, 2001; Conrad and
1004 Lithgow-Bertelloni, 2004; Copley et al., 2010), and the additional complication of continental ma-
1005 terial thought to be entering the subduction zone at the Seram Trench (Stevens et al., 2002), we
1006 have varied the force per unit length exerted on the Bird's Head by the Banda Arc between 10
1007 to -10×10^{12} N/m, where a positive value implies the force acts northeast and pushes the Bird's

1008 Head Block away from the Banda Arc, and a negative value implies the force acts southwest and
1009 pulls the BHB towards the subduction zone. For the Sorong-Yapen Fault Zone, we have modelled
1010 the shear force imparted onto the BHB by considering a shear stress between 1–30 MPa (similar
1011 to global earthquake stress drops; Allmann and Shearer, 2009) acting over a fault depth of 0–30
1012 km. This configuration generates a net shear force per unit length between $0.03\text{--}0.9 \times 10^{12}$ N/m
1013 along-strike. As the SFZ-YFZ is left-lateral, the shear force acts westwards upon the Bird’s Head
1014 Block.

1015

1016 Figure 14C-D shows the azimuth and magnitude of the resultant force required to balance
1017 the forces exerted upon the Bird’s Head Block, for each value of subduction zone and shear zone
1018 force per unit length. The azimuth represents the orientation of the force being exerted on the
1019 eastern margin of the Bird’s Head Block by central New Guinea, so an east-directed azimuth repre-
1020 sents extensional stress on the margin, and a north-directed azimuth represents left-lateral shear.
1021 The grey shading on Figure 14C-D shows the likely range of shear zone force per unit length,
1022 as discussed above. The purple shaded area shows the range of forces that are consistent with
1023 that shear zone force and also the required orientation of the resultant force given the orientation
1024 of left-lateral strike-slip and normal-faulting earthquakes along the margins of Cenderawasih Bay
1025 ($50\text{--}100^\circ$). This result shows that there is a plausible combination of forces from the Banda Arc
1026 and the Sorong-Yapen Fault Zone which could generate the observed faulting along the eastern
1027 margin of the Bird’s Head Block, and thus the increased curvature of the Banda Arc may have
1028 been responsible for the present-day tectonic configuration of western New Guinea.

1029

1030 The magnitude of the resultant force ($< 1.5 \times 10^{18}$ N), when averaged over a total fault length
1031 of ~ 600 km and a seismogenic thickness of 20 km, gives a stress estimate of < 125 MPa (with no
1032 lower bound). Our results also show that the magnitude of the force exerted by the Banda Arc on
1033 the Bird’s Head Block (subduction zone force) must be between $-2.8\text{--}0.3 \times 10^{12}$ N/m, with 50% of
1034 the models between $-2\text{--}0.2 \times 10^{12}$ N/m. If the seismogenic thickness of the Sorong and Yapen Shear
1035 Zones is reduced from 30 km to 20 km, the subduction zone force must be between $1.9\text{--}0.2 \times 10^{12}$

1036 N/m, with 50% of the models between $-1.3-0.1 \times 10^{12}$ N/m. Negative values for this subduction
1037 zone force, acting as a 'slab pull' force on the Bird's Head Block, are consistent with the existence
1038 of the Aru Trough: a ~ 3.5 km deep depression located south of the Bird's Head, where GPS data
1039 and earthquake focal mechanisms show that the trough is actively extending (Jacobson et al., 1979;
1040 Bock et al., 2003; Sloan and Jackson, 2012). Our estimates of the magnitude of the slab pull force
1041 from the Banda Arc ($0-2.8 \times 10^{12}$ N/m) are less than or equal to the values commonly inferred for
1042 other subduction zones ($2-2.5 \times 10^{12}$ N/m, Copley et al., 2010; $1-6 \times 10^{12}$ N/m, Capitanio et al.,
1043 2009; $8-40 \times 10^{12}$ N/m, Conrad and Lithgow-Bertelloni, 2002 and Conrad and Lithgow-Bertelloni,
1044 2004). Our estimates may be lower than most previous estimates of the magnitude of 'slab pull'
1045 because of the effects of positively buoyant continental material impinging on the subduction zone.

1046 7 Conclusions

1047 We have combined new earthquake source parameters with thermal modelling, analysis of gravity
1048 anomalies, and simple mechanical models in order to investigate the active and recent tectonics
1049 of New Guinea. We find that the pre-existing structural contrast across the Tasman Line in the
1050 Australian continental lithosphere plays an important role in controlling along-strike variations in
1051 the temperature structure, seismogenic thickness, and strength of the New Guinea foreland. These
1052 strength variations are reflected in the differing behaviour of the eastern foreland (where the crust
1053 appears broken through on high-angle faults) and the western foreland (where the crust appears
1054 mostly intact). Horizontal forces exerted between the New Guinea Highlands and forelands are
1055 estimated to be between $2\text{--}5 \times 10^{12}$ N/m along-strike. From these results, we are able to constrain
1056 the effective coefficient of friction on crustal faults within the foreland basin to be 0.01-0.28. The
1057 lack of correlation between foreland seismogenic thickness and the elevation of the New Guinea
1058 Highlands is likely to represent the time taken for the growth of topography to mirror the spatially-
1059 and temporally-varying strength of the bounding foreland, as the thinned passive margin of the
1060 northern Australian continent is consumed. Recent changes in the configuration of faulting in
1061 western New Guinea imply a changing tectonic force balance on that region, which is likely to be
1062 due to the progressive development of curvature in the Banda Arc.

1063 **8 Acknowledgements**

1064 We thank Simon Lamb and Laura Webb for insightful and constructive reviews. We also thank
1065 Domenico Chiarella and Robert Hall for helping with access to literature at Royal Holloway Uni-
1066 versity of London, James Jackson for useful comments on the manuscript, and Sam Wimpenny for
1067 assistance with coding. LK is supported by a Girdler Doctoral Scholarship. CB is supported by
1068 the Leverhulme grant 'Neptune' (RPG-2018-243).

1069 **9 Data availability**

1070 We have used several freely available datasets for topographic, earthquake, and gravity data.
1071 ETOPO2 (2-minute gridded global relief) data were downloaded from the NOAA National Centers
1072 for Environmental Information web page (<https://www.ngdc.noaa.gov/mgg/global/etopo2.html>).
1073 SRTM30 (30-metre resolution global relief) data were downloaded from within the Generic Map-
1074 ping Tools program (Wessel et al., 2019). Seismic waveforms were downloaded from the IRIS Data
1075 Management Centre (<https://ds.iris.edu/wilber3>). Additional earthquake source data were down-
1076 loaded from the Global CMT catalogue (<https://www.globalcmt.org>; Dziewonski et al., 1981; Ek-
1077 ström et al., 2012) and the ISC-EHB Bulletin (<http://www.isc.ac.uk/isc-ehb>; Weston et al., 2018;
1078 International Seismological Centre, 2020). GOCE free-air gravity anomalies were downloaded
1079 from the European Space Agency (<https://earth.esa.int/eogateway/missions/goce>). EIGEN-6C
1080 free-air gravity anomalies were downloaded from the International Centre for Global Earth Models
1081 (<http://icgem.gfz-potsdam.de>). All figures have been produced using Generic Mapping Tools v6
1082 (Wessel et al., 2019) and Inkscape v0.92.3 (Inkscape Project, 2018).

References

- Abers, Geoffrey and Robert McCaffrey (1988). “Active Deformation in the New Guinea Fold-and-Thrust Belt: Seismological Evidence for Strike-Slip Faulting and Basement-Involved Thrusting”. en. In: *Journal of Geophysical Research: Solid Earth* 93.B11, pp. 13332–13354. ISSN: 2156-2202. DOI: 10.1029/JB093iB11p13332.
- Abers, Geoffrey A. and Hélène Lyon-Caen (1990). “Regional Gravity Anomalies, Depth of the Foreland Basin and Isostatic Compensation of the New Guinea Highlands”. en. In: *Tectonics* 9.6, pp. 1479–1493. ISSN: 1944-9194. DOI: 10.1029/TC009i006p01479.
- Abers, Geoffrey A. and Steven W. Roecker (1991). “Deep Structure of an Arc-Continent Collision: Earthquake Relocation and Inversion for Upper Mantle P and S Wave Velocities beneath Papua New Guinea”. en. In: *Journal of Geophysical Research: Solid Earth* 96.B4, pp. 6379–6401. ISSN: 2156-2202. DOI: 10.1029/91JB00145.
- Aitchison, J. C., T. R. Ireland, M. C. Blake Jr., and P. G. Flood (1992). “530 Ma Zircon Age for Ophiolite from the New England Orogen: Oldest Rocks Known from Eastern Australia”. en. In: *Geology* 20.2, p. 125. ISSN: 0091-7613. DOI: 10.1130/0091-7613(1992)020<0125: MZAF0F>2.3.CO;2.
- Allmann, Bettina P. and Peter M. Shearer (2009). “Global Variations of Stress Drop for Moderate to Large Earthquakes”. en. In: *Journal of Geophysical Research: Solid Earth* 114.B1. ISSN: 2156-2202. DOI: 10.1029/2008JB005821.
- Artyushkov, E. V. (1973). “Stresses in the Lithosphere Caused by Crustal Thickness Inhomogeneities”. en. In: *Journal of Geophysical Research (1896-1977)* 78.32, pp. 7675–7708. ISSN: 2156-2202. DOI: 10.1029/JB078i032p07675.
- Assumpção, Marcelo and Gerardo Suárez (1988). “Source Mechanisms of Moderate-Size Earthquakes and Stress Orientation in Mid-Plate South America”. In: *Geophysical Journal International* 92.2, pp. 253–267. ISSN: 0956-540X. DOI: 10.1111/j.1365-246X.1988.tb01138.x.
- Babault, Julien, Marc Viaplana-Muzas, Xavier Legrand, Jean Van Den Driessche, Manuel González-Quijano, and Simon M. Mudd (2018). “Source-to-Sink Constraints on Tectonic and Sedimentary Evolution of the Western Central Range and Cenderawasih Bay (Indonesia)”. en. In: *Journal of Asian Earth Sciences* 156, pp. 265–287. ISSN: 13679120. DOI: 10.1016/j.jseaes.2018.02.004.
- Bailly, V., M. Pubellier, J.-C. Ringenbach, J. de Sigoyer, and F. Sapin (2009). “Deformation Zone ‘Jumps’ in a Young Convergent Setting; the Lengguru Fold-and-Thrust Belt, New Guinea Island”. en. In: *Lithos* 113.1-2, pp. 306–317. ISSN: 00244937. DOI: 10.1016/j.lithos.2009.08.013.
- Baldwin, Suzanne L., Paul G. Fitzgerald, and Laura E. Webb (2012). “Tectonics of the New Guinea Region”. en. In: *Annu. Rev. Earth Planet. Sci.* 40.1, pp. 495–520. ISSN: 0084-6597, 1545-4495. DOI: 10.1146/annurev-earth-040809-152540.

- Billen, Magali I. and Michael Gurnis (2001). “A Low Viscosity Wedge in Subduction Zones”. en. In: *Earth and Planetary Science Letters* 193.1-2, pp. 227–236. ISSN: 0012821X. DOI: 10.1016/S0012-821X(01)00482-4.
- Bock, Y., L. Prawirodirdjo, J. F. Genrich, C. W. Stevens, R. McCaffrey, C. Subarya, S. S. O. Puntodewo, and E. Calais (2003). “Crustal Motion in Indonesia from Global Positioning System Measurements”. en. In: *Journal of Geophysical Research: Solid Earth* 108.B8. ISSN: 2156-2202. DOI: 10.1029/2001JB000324.
- Bollinger, L., J. P. Avouac, R. Cattin, and M. R. Pandey (2004). “Stress Buildup in the Himalaya”. en. In: *Journal of Geophysical Research: Solid Earth* 109.B11. ISSN: 2156-2202. DOI: 10.1029/2003JB002911.
- Bouhifd, M. A., D. Andraut, G. Fiquet, and P. Richet (1996). “Thermal Expansion of Forsterite up to the Melting Point”. en. In: *Geophysical Research Letters* 23.10, pp. 1143–1146. ISSN: 1944-8007. DOI: 10.1029/96GL01118.
- Bourne, S. J., T. Árnadóttir, J. Beavan, D. J. Darby, P. C. England, B. Parsons, R. I. Walcott, and P. R. Wood (1998). “Crustal Deformation of the Marlborough Fault Zone in the South Island of New Zealand: Geodetic Constraints over the Interval 1982–1994”. en. In: *Journal of Geophysical Research: Solid Earth* 103.B12, pp. 30147–30165. ISSN: 2156-2202. DOI: 10.1029/98JB02228.
- Buchanan, Peter G. and John Warburton (1996). “The Influence of Pre-Existing Basin Architecture in the Development of the Papuan Fold and Thrust Belt: Implications for Petroleum Prospective”. en-US. In:
- Burov, E. B. (2010). “The Equivalent Elastic Thickness (T_e), Seismicity and the Long-Term Rheology of Continental Lithosphere: Time to Burn-out “Crème Brûlée”? Insights from Large-Scale Geodynamic Modeling”. en. In: *Tectonophysics. Quantitative Modelling of Geological Processes* 484.1, pp. 4–26. ISSN: 0040-1951. DOI: 10.1016/j.tecto.2009.06.013.
- Burov, E.B. and A.B. Watts (2006). “The Long-Term Strength of Continental Lithosphere: “Jelly Sandwich” or “Crème Brûlée”?” en. In: *GSA Today* 16.1, p. 4. ISSN: 1052-5173. DOI: 10.1130/1052-5173(2006)016<4:TLTSOC>2.0.CO;2.
- Byerlee, J. (1978). “Friction of Rocks”. en. In: *Rock Friction and Earthquake Prediction*. Ed. by James D. Byerlee and Max Wyss. Contributions to Current Research in Geophysics (CCRG). Basel: Birkhäuser, pp. 615–626. ISBN: 978-3-0348-7182-2. DOI: 10.1007/978-3-0348-7182-2_4.
- Capitanio, F. A., G. Morra, and S. Goes (2009). “Dynamics of Plate Bending at the Trench and Slab-Plate Coupling”. en. In: *Geochemistry, Geophysics, Geosystems* 10.4. ISSN: 1525-2027. DOI: 10.1029/2008GC002348.
- Cardwell, Richard K. and Bryan L. Isacks (1978). “Geometry of the Subducted Lithosphere beneath the Banda Sea in Eastern Indonesia from Seismicity and Fault Plane Solutions”. en. In: *Journal of Geophysical Research: Solid Earth* 83.B6, pp. 2825–2838. ISSN: 2156-2202. DOI: 10.1029/JB083iB06p02825.

- Carter, D. J., M. G. Audley-Charles, and A. J. Barber (1976). “Stratigraphical Analysis of Island Arc—Continental Margin Collision in Eastern Indonesia”. en. In: *Journal of the Geological Society* 132.2, pp. 179–198. ISSN: 0016-7649, 2041-479X. DOI: 10.1144/gsjgs.132.2.0179.
- Chapman, C. H, C Jen-Yi, D.G Lyness, and D.J Doornbos (1988). “The WKBJ Seismogram Algorithm”. In: *Seismological Algorithms: Computational Methods and Computer Programs*. Ed. by Doornbos, D.J., pp. 47–74.
- Charlton, Tim (1996). “Correlation of the Salawati and Tomori Basins, Eastern Indonesia: A Constraint on Left-Lateral Displacements of the Sorong Fault Zone”. In: *Geological Society, London, Special Publications* 106, pp. 465–481. DOI: 10.1144/GSL.SP.1996.106.01.29.
- Chen, Wang-Ping and Peter Molnar (1983). “Focal Depths of Intracontinental and Intraplate Earthquakes and Their Implications for the Thermal and Mechanical Properties of the Lithosphere”. en. In: *Journal of Geophysical Research: Solid Earth* 88.B5, pp. 4183–4214. ISSN: 2156-2202. DOI: 10.1029/JB088iB05p04183.
- Chen, Wang-Ping and Peter Molnar (1990). “Source Parameters of Earthquakes and Intraplate Deformation beneath the Shillong Plateau and the Northern Indoburman Ranges”. en. In: *Journal of Geophysical Research: Solid Earth* 95.B8, pp. 12527–12552. ISSN: 2156-2202. DOI: 10.1029/JB095iB08p12527.
- Clitheroe, G., O. Gudmundsson, and B. L. N. Kennett (2000). “The Crustal Thickness of Australia”. en. In: *Journal of Geophysical Research: Solid Earth* 105.B6, pp. 13697–13713. ISSN: 2156-2202. DOI: 10.1029/1999JB900317.
- Cloos, Mark, Benyamin Sapiie, Andrew Quarles van Ufford, Richard J. Weiland, Paul Q. Warren, and Timothy P. McMahon (2005). “Collisional Delamination in New Guinea: The Geotectonics of Subducting Slab Breakoff”. en. In: *Collisional Delamination in New Guinea: The Geotectonics of Subducting Slab Breakoff*. Geological Society of America. ISBN: 978-0-8137-2400-3. DOI: 10.1130/2005.2400.
- Coney, Peter J., Alaster Edwards, Richard Hine, Fiona Morrison, and Donal Windrim (1990). “The Regional Tectonics of the Tasman Orogenic System, Eastern Australia”. en. In: *Journal of Structural Geology*. Australasian Tectonics 12.5, pp. 519–543. ISSN: 0191-8141. DOI: 10.1016/0191-8141(90)90071-6.
- Conrad, Clinton P. and Bradford H. Hager (1999). “Effects of Plate Bending and Fault Strength at Subduction Zones on Plate Dynamics”. en. In: *Journal of Geophysical Research: Solid Earth* 104.B8, pp. 17551–17571. ISSN: 2156-2202. DOI: 10.1029/1999JB900149.
- Conrad, Clinton P. and Carolina Lithgow-Bertelloni (2002). “How Mantle Slabs Drive Plate Tectonics”. en. In: *Science* 298.5591, pp. 207–209. ISSN: 0036-8075, 1095-9203. DOI: 10.1126/science.1074161.
- Conrad, Clinton P. and Carolina Lithgow-Bertelloni (2004). “The Temporal Evolution of Plate Driving Forces: Importance of “Slab Suction” versus “Slab Pull” during the Cenozoic”. en.

- In: *Journal of Geophysical Research: Solid Earth* 109.B10. ISSN: 2156-2202. DOI: 10.1029/2004JB002991.
- Copley, Alex, Jean-Philippe Avouac, James Hollingsworth, and Sébastien Leprince (2011). “The 2001 Mw 7.6 Bhuj Earthquake, Low Fault Friction, and the Crustal Support of Plate Driving Forces in India”. en. In: *Journal of Geophysical Research: Solid Earth* 116.B8. ISSN: 2156-2202. DOI: 10.1029/2010JB008137.
- Copley, Alex, Jean-Philippe Avouac, and Jean-Yves Royer (2010). “India-Asia Collision and the Cenozoic Slowdown of the Indian Plate: Implications for the Forces Driving Plate Motions”. en. In: *Journal of Geophysical Research* 115.B3. ISSN: 0148-0227. DOI: 10.1029/2009JB006634.
- Copley, Alex, Fran Boait, James Hollingsworth, James Jackson, and Dan McKenzie (2009). “Sub-parallel Thrust and Normal Faulting in Albania and the Roles of Gravitational Potential Energy and Rheology Contrasts in Mountain Belts”. en. In: *Journal of Geophysical Research* 114.B5. ISSN: 0148-0227. DOI: 10.1029/2008JB005931.
- Copley, Alex and Nigel Woodcock (2016). “Estimates of Fault Strength from the Variscan Foreland of the Northern UK”. en. In: *Earth and Planetary Science Letters* 451, pp. 108–113. ISSN: 0012-821X. DOI: 10.1016/j.epsl.2016.07.024.
- Craig, T. J. and J. A. Jackson (2021). “Variations in the Seismogenic Thickness of East Africa”. en. In: *Journal of Geophysical Research: Solid Earth* 126.3. e2020JB020754 2020JB020754, e2020JB020754. ISSN: 2169-9356. DOI: 10.1029/2020JB020754.
- Craig, T. J., J. A. Jackson, K. Priestley, and D. McKenzie (2011). “Earthquake Distribution Patterns in Africa: Their Relationship to Variations in Lithospheric and Geological Structure, and Their Rheological Implications: Earthquake Distribution Patterns in Africa”. en. In: *Geophysical Journal International* 185.1, pp. 403–434. ISSN: 0956540X. DOI: 10.1111/j.1365-246X.2011.04950.x.
- Craig, T. J., P. B. Kelemen, B. R. Hacker, and A. Copley (2020). “Reconciling Geophysical and Petrological Estimates of the Thermal Structure of Southern Tibet”. en. In: *Geochemistry, Geophysics, Geosystems* 21.8. e2019GC008837 10.1029/2019GC008837, e2019GC008837. ISSN: 1525-2027. DOI: 10.1029/2019GC008837.
- Crawford, A., Sebastien Meffre, and P. Symonds (2003). “120 to 0 Ma Tectonic Evolution of the Southwest Pacific and Analogous Geological Evolution of the 600 to 220 Ma Tasman Fold Belt System”. In: *Geol. Soc. Australia Spec. Publ.* Vol. 22, pp. 383–403. ISBN: 978-0-8137-2372-3. DOI: 10.1130/0-8137-2372-8.383.
- Daczko, Nathan R., Peter Caffi, and Paul Mann (2011). “Structural Evolution of the Dayman Dome Metamorphic Core Complex, Eastern Papua New Guinea”. en. In: *GSA Bulletin* 123.11-12, pp. 2335–2351. ISSN: 0016-7606. DOI: 10.1130/B30326.1.
- Dalmayrac, Bernard and Peter Molnar (1981). “Parallel Thrust and Normal Faulting in Peru and Constraints on the State of Stress”. en. In: *Earth and Planetary Science Letters* 55.3, pp. 473–481. ISSN: 0012-821X. DOI: 10.1016/0012-821X(81)90174-6.

- Davies, H L, R C B Perembol, R D Winn, and P KenGemar (1997). “Terranes of the New Guinea Orogen”. en. In: p. 7.
- Davies, H. L. and A. L. Jaques (1984). “Emplacement of Ophiolite in Papua New Guinea”. en. In: *Geological Society, London, Special Publications* 13.1, pp. 341–349. ISSN: 0305-8719, 2041-4927. DOI: 10.1144/GSL.SP.1984.013.01.27.
- Davies, Hugh L. (2012). “The Geology of New Guinea - the Cordilleran Margin of the Australian Continent”. en. In: *Episodes Journal of International Geoscience* 35.1, pp. 87–102. DOI: 10.18814/epiugs/2012/v35i1/008.
- de Sigoyer, Julia, Camille François, Alain Cocherie, Manuel Pubellier, Vivien Bailly, and Jean Claude Ringenbach (2011). “Very Young and Fast Exhumation, between 8 and 5 Ma, for the High Pressure Metasediments of Lengguru Prism, W-Papua”. en. In:
- Decker, John, Steven Bergman, Philip Teas, and D.L. Orange (2009). “Constraints on the Tectonic Evolution of the Bird’s Head, West Papua, Indonesia”. In: *Indonesian Petroleum Association, 33rd Annual Convention and Exhibition*. DOI: 10.29118/IPA.556.09.G.139.
- DeMets, Charles, Richard G. Gordon, Donald F. Argus, and Seth Stein (1994). “Effect of Recent Revisions to the Geomagnetic Reversal Time Scale on Estimates of Current Plate Motions”. en. In: *Geophysical Research Letters* 21.20, pp. 2191–2194. ISSN: 1944-8007. DOI: 10.1029/94GL02118.
- Devlin, S., B. L. Isacks, M. E. Pritchard, W. D. Barnhart, and R. B. Lohman (2012). “Depths and Focal Mechanisms of Crustal Earthquakes in the Central Andes Determined from Teleseismic Waveform Analysis and InSAR”. en. In: *Tectonics* 31.2. ISSN: 1944-9194. DOI: 10.1029/2011TC002914.
- Dow, D.B. and R. Sukanto (1984). “Western Irian Jaya: The End-Product of Oblique Plate Convergence in the Late Tertiary”. en. In: *Tectonophysics* 106.1-2, pp. 109–139. ISSN: 00401951. DOI: 10.1016/0040-1951(84)90224-5.
- Drinkwater, M, R. Haagmans, D. Muzi, A. Popescu, Rune Floberghagen, Michael Kern, and M. Fehringer (2007). “The GOCE Gravity Mission: ESA’s First Core Explorer”. In: *Proceedings of 3rd International GOCE User Workshop*.
- Dziewonski, A. M., T.-A. Chou, and J. H. Woodhouse (1981). “Determination of Earthquake Source Parameters from Waveform Data for Studies of Global and Regional Seismicity”. en. In: *Journal of Geophysical Research: Solid Earth* 86.B4, pp. 2825–2852. ISSN: 2156-2202. DOI: 10.1029/JB086iB04p02825.
- Ekström, G., M. Nettles, and A.M. Dziewoński (2012). “The Global CMT Project 2004–2010: Centroid-Moment Tensors for 13,017 Earthquakes”. en. In: *Physics of the Earth and Planetary Interiors* 200-201, pp. 1–9. ISSN: 00319201. DOI: 10.1016/j.pepi.2012.04.002.
- Engdahl, E. Robert, Rob van der Hilst, and Raymond Buland (1998). “Global Teleseismic Earthquake Relocation with Improved Travel Times and Procedures for Depth Determination”. en. In: *Bulletin of the Seismological Society of America* 88.3, pp. 722–743. ISSN: 0037-1106.

- Engdahl, Robert E., James A. Jackson, Stephen C. Myers, Eric A. Bergman, and Keith Priestley (2006). “Relocation and Assessment of Seismicity in the Iran Region”. en. In: *Geophysical Journal International* 167.2, pp. 761–778. ISSN: 0956540X, 1365246X. DOI: 10.1111/j.1365-246X.2006.03127.x.
- England, Philip and Gregory Houseman (1989). “Extension during Continental Convergence, with Application to the Tibetan Plateau”. en. In: *Journal of Geophysical Research: Solid Earth* 94.B12, pp. 17561–17579. ISSN: 2156-2202. DOI: 10.1029/JB094iB12p17561.
- England, Philip and Dan McKenzie (1982). “A Thin Viscous Sheet Model for Continental Deformation”. en. In: *Geophysical Journal of the Royal Astronomical Society* 70.2, pp. 295–321. ISSN: 1365-246X. DOI: 10.1111/j.1365-246X.1982.tb04969.x.
- England, Philip and Peter Molnar (2015). “Rheology of the Lithosphere beneath the Central and Western Tien Shan”. en. In: *Journal of Geophysical Research: Solid Earth* 120.5, pp. 3803–3823. ISSN: 2169-9356. DOI: 10.1002/2014JB011733.
- England, Philip Christopher and G. A. Houseman (1988). “The Mechanics of the Tibetan Plateau”. In: *Philosophical Transactions of the Royal Society of London. Series A, Mathematical and Physical Sciences* 326.1589, pp. 301–320. DOI: 10.1098/rsta.1988.0089.
- Farr, Tom G., Paul A. Rosen, Edward Caro, Robert Crippen, Riley Duren, Scott Hensley, Michael Kobrick, Mimi Paller, Ernesto Rodriguez, Ladislav Roth, David Seal, Scott Shaffer, Joanne Shimada, Jeffrey Umland, Marian Werner, Michael Oskin, Douglas Burbank, and Douglas Alsdorf (2007). “The Shuttle Radar Topography Mission”. en. In: *Reviews of Geophysics* 45.2. ISSN: 1944-9208. DOI: 10.1029/2005RG000183.
- Förste, Christoph, Sean Bruinsma, Oleg Abrikosov, Frank Flechtner, Jean-Charles Marty, Jean-Michel Lemoine, Christoph Dahle, Hans Neumayer, Franz Barthelmes, Rolf König, and Richard Biancale (2014). “EIGEN-6C4 - The Latest Combined Global Gravity Field Model Including GOCE Data up to Degree and Order 1949 of GFZ Potsdam and GRGS Toulouse”. In: *EGU General Assembly Conference Abstracts*. Vol. 16, p. 3707.
- Forsyth, D. and S. Uyeda (1975). “On the Relative Importance of the Driving Forces of Plate Motion”. en. In: *Geophysical Journal International* 43.1, pp. 163–200. ISSN: 0956-540X, 1365-246X. DOI: 10.1111/j.1365-246X.1975.tb00631.x.
- François, Camille, Julia de Sigoyer, Manuel Pubellier, Vivien Bailly, Alain Cocherie, and Jean-Claude Ringenbach (2016). “Short-Lived Subduction and Exhumation in Western Papua (Wandamen Peninsula): Co-Existence of HP and HT Metamorphic Rocks in a Young Geodynamic Setting”. en. In: *Lithos* 266-267, pp. 44–63. ISSN: 00244937. DOI: 10.1016/j.lithos.2016.09.030.
- Gaina, Carmen, R. Dietmar Müller, Jean-Yves Royer, and Phil Symonds (1999). “Evolution of the Louisiade Triple Junction”. en. In: *Journal of Geophysical Research: Solid Earth* 104.B6, pp. 12927–12939. ISSN: 2156-2202. DOI: 10.1029/1999JB900038.

- Glen, R. A. (2005). “The Tasmanides of Eastern Australia”. en. In: *Geological Society, London, Special Publications* 246.1, pp. 23–96. ISSN: 0305-8719, 2041-4927. DOI: 10.1144/GSL.SP.2005.246.01.02.
- Granath, J.W, K Soofi, and J.B Mercer (1991). “Applications of SAR in Structural Modeling of the Central Ranges Thrust Belt, Irian Jaya, Indonesia”. In: *Thematic Conference on Geologic Remote Sensing*. Denver, CO.
- Haddad, D. and A. B. Watts (1999). “Subsidence History, Gravity Anomalies, and Flexure of the Northeast Australian Margin in Papua New Guinea”. en. In: *Tectonics* 18.5, pp. 827–842. ISSN: 1944-9194. DOI: 10.1029/1999TC900009.
- Hall, Robert (2002). “Cenozoic Geological and Plate Tectonic Evolution of SE Asia and the SW Pacific: Computer-Based Reconstructions, Model and Animations”. en. In: *Journal of Asian Earth Sciences*. Cenozoic Geological and Plate Tectonic Evolution of SE Asia and the SW Pacific: Computer-Based Reconstructions, Model and Animations (Including CD-ROM) 20.4, pp. 353–431. ISSN: 1367-9120. DOI: 10.1016/S1367-9120(01)00069-4.
- Hamilton, P. J., R. W. Johnson, D. E. Mackenzie, and R. K. O’Nions (1983). “Pleistocene Volcanic Rocks from the Fly-Highlands Province of Western Papua New Guinea: A Note on New Sr and Nd Isotopic Data and Their Petrogenetic Implications”. en. In: *Journal of Volcanology and Geothermal Research* 18.1, pp. 449–459. ISSN: 0377-0273. DOI: 10.1016/0377-0273(83)90020-3.
- Hamilton, Warren (1979). *Tectonics of the Indonesian Region*. en. Vol. 1078. US Government Printing Office.
- Hasterok, D., M. Gard, and J. Webb (2018). “On the Radiogenic Heat Production of Metamorphic, Igneous, and Sedimentary Rocks”. en. In: *Geoscience Frontiers*. Reliability Analysis of Geotechnical Infrastructures 9.6, pp. 1777–1794. ISSN: 1674-9871. DOI: 10.1016/j.gsf.2017.10.012.
- Herman, Frédéric, Peter Copeland, Jean-Philippe Avouac, Laurent Bollinger, Gweltaz Mahéo, Patrick Le Fort, Santaman Rai, David Foster, Arnaud Pêcher, Kurt Stüwe, and Pierre Henry (2010). “Exhumation, Crustal Deformation, and Thermal Structure of the Nepal Himalaya Derived from the Inversion of Thermochronological and Thermobarometric Data and Modeling of the Topography”. en. In: *Journal of Geophysical Research: Solid Earth* 115.B6. ISSN: 2156-2202. DOI: 10.1029/2008JB006126.
- Hill, K. C. and R. Hall (2003). “Mesozoic-Cenozoic Evolution of Australia’s New Guinea Margin in a West Pacific Context”. en. In: *Evolution and Dynamics of the Australian Plate*. Geological Society of America. ISBN: 978-0-8137-2372-3. DOI: 10.1130/0-8137-2372-8.265.
- Hill, KC (1991). “Structure of the Papuan Fold Belt, Papua New Guinea”. In: *AAPG Bulletin* 75.5, pp. 857–872. ISSN: 0149-1423. DOI: 10.1306/OC9B2871-1710-11D7-8645000102C1865D.
- Hill, Kevin C. and Asaf Raza (1999). “Arc-Continent Collision in Papua Guinea: Constraints from Fission Track Thermochronology”. en. In: *Tectonics* 18.6, pp. 950–966. ISSN: 1944-9194. DOI: 10.1029/1999TC900043.

- Hinschberger, Florent, Jacques-André Malod, Jean-Pierre Réhault, Michel Villeneuve, Jean-Yves Royer, and Safri Burhanuddin (2005). “Late Cenozoic Geodynamic Evolution of Eastern Indonesia”. en. In: *Tectonophysics* 404.1, pp. 91–118. ISSN: 0040-1951. DOI: 10.1016/j.tecto.2005.05.005.
- Hobson, D. M. (1986). “A THIN SKINNED MODEL FOR THE PAPUAN THRUST BELT AND SOME IMPLICATIONS FOR HYDROCARBON EXPLORATION”. en. In: *The APPEA Journal* 26.1, pp. 214–225. ISSN: 2206-8996. DOI: 10.1071/aj85021.
- Hofmeister, A. M. (1999). “Mantle Values of Thermal Conductivity and the Geotherm from Phonon Lifetimes”. en. In: *Science* 283.5408, pp. 1699–1706. ISSN: 00368075, 10959203. DOI: 10.1126/science.283.5408.1699.
- Imber, J., R. E. Holdsworth, S. a. F. Smith, S. P. Jefferies, and C. Collettini (2008). “Frictional-Viscous Flow, Seismicity and the Geology of Weak Faults: A Review and Future Directions”. en. In: *Geological Society, London, Special Publications* 299.1, pp. 151–173. ISSN: 0305-8719, 2041-4927. DOI: 10.1144/SP299.10.
- Inkscape Project (2018). *Inkscape v0.92.3*. Inkscape v0.92.3. <https://inkscape.org>.
- International Seismological Centre (2020). “ISC-EHB Dataset”. In: DOI: doi.org/10.31905/PY08W6S3.
- Jackson, J. A. and N. J. White (1989). “Normal Faulting in the Upper Continental Crust: Observations from Regions of Active Extension”. en. In: *Journal of Structural Geology* 11.1, pp. 15–36. ISSN: 0191-8141. DOI: 10.1016/0191-8141(89)90033-3.
- Jackson, James, Dan McKenzie, and Keith Priestley (2021). “Relations between Earthquake Distributions, Geological History, Tectonics and Rheology on the Continents”. en. In: *Phil. Trans. R. Soc. A* 379.2193, p. 20190412. ISSN: 1364-503X, 1471-2962. DOI: 10.1098/rsta.2019.0412.
- Jackson, James, Dan McKenzie, Keith Priestley, and Brian Emmerson (2008). “New Views on the Structure and Rheology of the Lithosphere”. en. In: *Journal of the Geological Society* 165.2, pp. 453–465. ISSN: 0016-7649, 2041-479X. DOI: 10.1144/0016-76492007-109.
- Jacobson, R. S., G. G. Shor Jr, R. M. Kieckhefer, and G. M. Purdy (1979). “Seismic Refraction and Reflection Studies in the Timor-Aru Trough System and Australian Continental Shelf: Convergent Margins”. en-US. In: 109, pp. 209–222.
- Jaupart, C, S Labrosse, F Lucazeau, and J.-C Mareschal (2015). “Temperatures, Heat, and Energy in the Mantle of the Earth”. In: *Treatise on Geophysics*. Second. Vol. 7, pp. 223–270.
- Johnson, R. W., D. E. Mackenzie, and I. E. M. Smith (1978). “Delayed Partial Melting of Subduction-Modified Mantle in Papua New Guinea”. en. In: *Tectonophysics* 46.1, pp. 197–216. ISSN: 0040-1951. DOI: 10.1016/0040-1951(78)90114-2.
- Jost, Benjamin M., Max Webb, and Lloyd T. White (2018). “The Mesozoic and Palaeozoic Granitoids of North-Western New Guinea”. en. In: *Lithos* 312-313, pp. 223–243. ISSN: 0024-4937. DOI: 10.1016/j.lithos.2018.04.027.

- Karato, S.-i. and P. Wu (1993). “Rheology of the Upper Mantle: A Synthesis”. en. In: *Science* 260.5109, pp. 771–778. ISSN: 0036-8075, 1095-9203. DOI: 10.1126/science.260.5109.771.
- Kayal, J R and Dapeng Zhao (1998). “Three-Dimensional Seismic Structure beneath Shillong Plateau and Assam Valley, Northeast India”. en. In: *Bulletin of the Seismological Society of America*, p. 10.
- Kennett, B. L. N., E. R. Engdahl, and R. Buland (1995). “Constraints on Seismic Velocities in the Earth from Traveltimes”. en. In: *Geophysical Journal International* 122.1, pp. 108–124. ISSN: 0956540X, 1365246X. DOI: 10.1111/j.1365-246X.1995.tb03540.x.
- Kohlstedt, D. L., Brian Evans, and S. J. Mackwell (1995). “Strength of the Lithosphere: Constraints Imposed by Laboratory Experiments”. en. In: *Journal of Geophysical Research: Solid Earth* 100.B9, pp. 17587–17602. ISSN: 2156-2202. DOI: 10.1029/95JB01460.
- Koulali, A., P. Tregoning, S. McClusky, R. Stanaway, L. Wallace, and G. Lister (2015). “New Insights into the Present-Day Kinematics of the Central and Western Papua New Guinea from GPS”. en. In: *Geophysical Journal International* 202.2, pp. 993–1004. ISSN: 1365-246X, 0956-540X. DOI: 10.1093/gji/ggv200.
- Kumar, Ajay, Supriyo Mitra, and G. Suresh (2015). “Seismotectonics of the Eastern Himalayan and Indo-Burman Plate Boundary Systems”. en. In: *Tectonics* 34.11, pp. 2279–2295. ISSN: 1944-9194. DOI: 10.1002/2015TC003979.
- Lamb, Simon (2006). “Shear Stresses on Megathrusts: Implications for Mountain Building behind Subduction Zones”. en. In: *Journal of Geophysical Research: Solid Earth* 111.B7. ISSN: 2156-2202. DOI: 10.1029/2005JB003916.
- Lamb, Simon, James D. P. Moore, Marta Perez-Gussinye, and Tim Stern (2020). “Global Whole Lithosphere Isostasy: Implications for Surface Elevations, Structure, Strength, and Densities of the Continental Lithosphere”. en. In: *Geochemistry, Geophysics, Geosystems* 21.10. e2020GC009150 2020GC009150, e2020GC009150. ISSN: 1525-2027. DOI: 10.1029/2020GC009150.
- Lockner, David A., Carolyn Morrow, Diane Moore, and Stephen Hickman (2011). “Low Strength of Deep San Andreas Fault Gouge from SAFOD Core”. en. In: *Nature* 472.7341, pp. 82–85. ISSN: 1476-4687. DOI: 10.1038/nature09927.
- Lund, Mats G., Håkon Austrheim, and Muriel Erambert (2004). “Earthquakes in the Deep Continental Crust - Insights from Studies on Exhumed High-Pressure Rocks”. en. In: *Geophysical Journal International* 158.2, pp. 569–576. ISSN: 0956540X, 1365246X. DOI: 10.1111/j.1365-246X.2004.02368.x.
- Mackwell, S. J., M. E. Zimmerman, and D. L. Kohlstedt (1998). “High-Temperature Deformation of Dry Diabase with Application to Tectonics on Venus”. en. In: *Journal of Geophysical Research: Solid Earth* 103.B1, pp. 975–984. ISSN: 2156-2202. DOI: 10.1029/97JB02671.
- Maggi, A., J. A. Jackson, K. Priestley, and C. Baker (2000a). “A Re-assessment of Focal Depth Distributions in Southern Iran, the Tien Shan and Northern India: Do Earthquakes Really

- Occur in the Continental Mantle?” In: *Geophysical Journal International* 143.3, pp. 629–661. ISSN: 0956-540X. DOI: 10.1046/j.1365-246X.2000.00254.x.
- Maggi, A., J.A. Jackson, D. McKenzie, and K. Priestley (2000b). “Earthquake Focal Depths, Effective Elastic Thickness, and the Strength of the Continental Lithosphere”. In: *Geology* 28.6, pp. 495–498. ISSN: 0091-7613. DOI: 10.1130/0091-7613(2000)28<495:EFDEET>2.0.CO;2.
- McCaffrey, Robert (1989). “Seismological Constraints and Speculations on Banda Arc Tectonics”. en. In: *Netherlands Journal of Sea Research* 24.2, pp. 141–152. ISSN: 0077-7579. DOI: 10.1016/0077-7579(89)90145-2.
- McCaffrey, Robert (1996). “Slip Partitioning at Convergent Plate Boundaries of SE Asia”. en. In: *Geological Society, London, Special Publications* 106.1, pp. 3–18. ISSN: 0305-8719, 2041-4927. DOI: 10.1144/GSL.SP.1996.106.01.02.
- McCaffrey, Robert, G. Abers, and P. Zwick (1991). “Inversion of Teleseismic Body Waves”. In: *IASPEI Software library* 3, pp. 81–166.
- McCaffrey, Robert and Geoffrey Abers (1988). *SYN3: A Program for Inversion of Teleseismic Body Wave Forms on Microcomputers*: en. Tech. rep. Fort Belvoir, VA: Defense Technical Information Center. DOI: 10.21236/ADA198940.
- McCaffrey, Robert and Geoffrey A. Abers (1991). “Orogeny in Arc-Continent Collision: The Banda Arc and Western New Guinea”. en. In: *Geology* 19.6, pp. 563–566. ISSN: 0091-7613. DOI: 10.1130/0091-7613(1991)019<0563:0IACCT>2.3.CO;2.
- McDowell, Fred W., Timothy P. McMahon, Paul Q. Warren, and Mark Cloos (1996). “Pliocene Cu-Au-Bearing Igneous Intrusions of the Gunung Bijih (Ertsberg) District, Irian Jaya, Indonesia: K-Ar Geochronology”. In: *The Journal of Geology* 104.3, pp. 327–340. ISSN: 0022-1376. DOI: 10.1086/629828.
- McKenzie, Dan and Derek Fairhead (1997). “Estimates of the Effective Elastic Thickness of the Continental Lithosphere from Bouguer and Free Air Gravity Anomalies”. en. In: *Journal of Geophysical Research: Solid Earth* 102.B12, pp. 27523–27552. ISSN: 2156-2202. DOI: 10.1029/97JB02481.
- McKenzie, Dan, James Jackson, and Keith Priestley (2005). “Thermal Structure of Oceanic and Continental Lithosphere”. en. In: *Earth and Planetary Science Letters* 233.3, pp. 337–349. ISSN: 0012-821X. DOI: 10.1016/j.epsl.2005.02.005.
- McKenzie, Dan, Weiyong Yi, and Reiner Rummel (2014). “Estimates of T_e from GOCE Data”. en. In: *Earth and Planetary Science Letters* 399, pp. 116–127. ISSN: 0012821X. DOI: 10.1016/j.epsl.2014.05.003.
- McKenzie, Dan, Weiyong Yi, and Reiner Rummel (2015). “Estimates of T_e for Continental Regions Using GOCE Gravity”. en. In: *Earth and Planetary Science Letters* 428, pp. 97–107. ISSN: 0012-821X. DOI: 10.1016/j.epsl.2015.07.036.

- Mei, S., A. M. Suzuki, D. L. Kohlstedt, N. A. Dixon, and W. B. Durham (2010). “Experimental Constraints on the Strength of the Lithospheric Mantle”. en. In: *Journal of Geophysical Research: Solid Earth* 115.B8. ISSN: 2156-2202. DOI: 10.1029/2009JB006873.
- Miao, S. Q., H. P. Li, and G. Chen (2014). “Temperature Dependence of Thermal Diffusivity, Specific Heat Capacity, and Thermal Conductivity for Several Types of Rocks”. en. In: *J Therm Anal Calorim* 115.2, pp. 1057–1063. ISSN: 1588-2926. DOI: 10.1007/s10973-013-3427-2.
- Mitra, S., K. F. Priestley, Kajaljyoti Borah, and V. K. Gaur (2018). “Crustal Structure and Evolution of the Eastern Himalayan Plate Boundary System, Northeast India”. en. In: *Journal of Geophysical Research: Solid Earth* 123.1, pp. 621–640. ISSN: 2169-9356. DOI: 10.1002/2017JB014714.
- Moffat, D. T., L. F. Henage, R. A. Brash, R. W. Tauer, and B. H. Harahap (1991). “Lengguru, Irian Jaya: Prospect Selection Using Field Mapping, Balanced Cross-Sections, and Gravity Modelling”. en-US. In: pp. 85–106.
- Molnar, P. and Hélène Lyon-Caen (1988). “Some Simple Physical Aspects of the Support, Structure, and Evolution of Mountain Belts”. In: *Processes in Continental Lithospheric Deformation*, pp. 179–207.
- Molnar, Peter and Hélène Lyon-Caen (1989). “Fault Plane Solutions of Earthquakes and Active Tectonics of the Tibetan Plateau and Its Margins”. en. In: *Geophysical Journal International* 99.1, pp. 123–154. ISSN: 0956540X, 1365246X. DOI: 10.1111/j.1365-246X.1989.tb02020.x.
- Moore, Clive (2003). *New Guinea: Crossing Boundaries and History*. en. University of Hawaii Press. ISBN: 978-0-8248-2485-3.
- Nash, C. R., G. Artmont, M. L. Gillan, D. Lennie, G. O’Connor, and K. R. Parris (1993). “Structure of the Irian Jaya Mobile Belt, Irian Jaya, Indonesia”. en. In: *Tectonics* 12.2, pp. 519–535. ISSN: 1944-9194. DOI: 10.1029/92TC02360.
- Nemati, Majid, James Hollingsworth, Zhongwen Zhan, Mohammad Javad Bolourchi, and Morteza Talebian (2013). “Microseismicity and Seismotectonics of the South Caspian Lowlands, NE Iran”. In: *Geophysical Journal International* 193.3, pp. 1053–1070. ISSN: 0956-540X. DOI: 10.1093/gji/ggs114.
- Nissen, Edwin, Mohammad Tatar, James A. Jackson, and Mark B. Allen (2011). “New Views on Earthquake Faulting in the Zagros Fold-and-Thrust Belt of Iran: Earthquake Faulting in the Zagros”. en. In: *Geophysical Journal International* 186.3, pp. 928–944. ISSN: 0956540X. DOI: 10.1111/j.1365-246X.2011.05119.x.
- Pérez-Gussinyé, M., A. R. Lowry, and A. B. Watts (2007). “Effective Elastic Thickness of South America and Its Implications for Intracontinental Deformation”. en. In: *Geochemistry, Geophysics, Geosystems* 8.5. ISSN: 1525-2027. DOI: 10.1029/2006GC001511.
- Pieters, P. E., C. J. Pigram, D. S. Trail, D. B. Dow, N. Ratman, and R. Sukamto (1983). “The Stratigraphy of Western Irian Jaya”. en-US. In: pp. 229–261.

- Pigram, C. J., P. J. Davies, D. A. Feary, and P. A. Symonds (1989). “Tectonic Controls on Carbonate Platform Evolution in Southern Papua New Guinea: Passive Margin to Foreland Basin”. en. In: *Geology* 17.3, pp. 199–202. ISSN: 0091-7613. DOI: 10.1130/0091-7613(1989)017<0199:TCOCPE>2.3.CO;2.
- Pigram, C. J. and H. Panggabean (1984). “Rifting of the Northern Margin of the Australian Continent and the Origin of Some Microcontinents in Eastern Indonesia”. en. In: *Tectonophysics* 107.3, pp. 331–353. ISSN: 0040-1951. DOI: 10.1016/0040-1951(84)90257-9.
- Pigram, C.J. and P.A. Symonds (1991). “A Review of the Timing of the Major Tectonic Events in the New Guinea Orogen”. en. In: *Journal of Southeast Asian Earth Sciences* 6.3-4, pp. 307–318. ISSN: 07439547. DOI: 10.1016/0743-9547(91)90076-A.
- Plumb, K. A. (1979). “The Tectonic Evolution of Australia”. en. In: *Earth-Science Reviews* 14.3, pp. 205–249. ISSN: 0012-8252. DOI: 10.1016/0012-8252(79)90001-1.
- Press, W.H., S.A. Teukolsky, W.T. Vetterling, and B.P. Flannery (1992). *Numerical Recipes: The Art of Scientific Computing*. Second. Cambridge University Press.
- Priastomo, Yasinto S. (2012). “Tectonostratigraphy Evolution of Cendrawasih Bay Basin Papua, Indonesia”. MSc Thesis. Royal Holloway University of London.
- Priestley, Keith, James Jackson, and Dan McKenzie (2008). “Lithospheric Structure and Deep Earthquakes beneath India, the Himalaya and Southern Tibet”. In: *Geophysical Journal International* 172.1, pp. 345–362. ISSN: 0956-540X. DOI: 10.1111/j.1365-246X.2007.03636.x.
- Priestley, Keith, Dan McKenzie, and Tak Ho (2018). “A Lithosphere–Asthenosphere Boundary—a Global Model Derived from Multimode Surface-Wave Tomography and Petrology”. en. In: *Lithospheric Discontinuities*. American Geophysical Union (AGU), pp. 111–123. ISBN: 978-1-119-24974-0.
- Pubellier, Manuel and Frédéric Ego (2002). “Anatomy of an Escape Tectonic Zone: Western Irian Jaya (Indonesia)”. en. In: *Tectonics* 21.4, pp. 1-1-1–16. ISSN: 1944-9194. DOI: 10.1029/2001TC901038.
- Puntodewo, S.S.O., R. McCaffrey, E. Calais, Y. Bock, J. Rais, C. Subarya, R. Poewariardi, C. Stevens, J. Genrich, Fauzi, P. Zwick, and S. Wdowinski (1994). “GPS Measurements of Crustal Deformation within the Pacific-Australia Plate Boundary Zone in Irian Jaya, Indonesia”. en. In: *Tectonophysics* 237.3-4, pp. 141–153. ISSN: 00401951. DOI: 10.1016/0040-1951(94)90251-8.
- Remitti, F., S. a. F. Smith, S. Mitterpergher, A. F. Gualtieri, and G. Di Toro (2015). “Frictional Properties of Fault Zone Gouges from the J-FAST Drilling Project (Mw 9.0 2011 Tohoku-Oki Earthquake)”. en. In: *Geophysical Research Letters* 42.8, pp. 2691–2699. ISSN: 1944-8007. DOI: 10.1002/2015GL063507.
- Royer, Jean-Yves and David T. Sandwell (1989). “Evolution of the Eastern Indian Ocean since the Late Cretaceous: Constraints from Geosat Altimetry”. en. In: *Journal of Geophysical Research: Solid Earth* 94.B10, pp. 13755–13782. ISSN: 2156-2202. DOI: 10.1029/JB094iB10p13755.

- Rudnick, Roberta and A.A. Nyblade (1999). “The Thickness and Heat Production of Archean Lithosphere, Constraints from Xenolith Thermobarometry and Surface Heat Flow”. In: *mantle petrology: field observations and high-pressure experimentation: a tribute to Francis R. Boyd, geochemical Soc. spec.* 6, pp. 3–12.
- Rudnick, Roberta L., William F. McDonough, and Richard J. O’Connell (1998). “Thermal Structure, Thickness and Composition of Continental Lithosphere”. en. In: *Chemical Geology* 145.3-4, pp. 395–411. ISSN: 00092541. DOI: 10.1016/S0009-2541(97)00151-4.
- Sapiie, Benyamin, A. C. Adyagharini, and Phillips Teas (2010). “New Insight of Tectonic Evolution of Cendrawasih Bay and Its Implications for Hydrocarbon Prospect, Papua, Indonesia”. en-US. In: *Indonesian Petroleum Association, 34th Annual Convention and Exhibition*. Indonesian Petroleum Association.
- Schiebner, E (1974). “Fossil Fracture Zones (Transform Faults), Segmentation and Correlation Problems in the Tasman Fold Belt System.” In: *The Tasman Geosyncline—A Symposium in Honour of Professor Dorothy Hill, Queensland Division Geological Society of Australia, Brisbane*, pp. 65–96.
- Scholz, Christopher H. (1982). “Scaling Laws for Large Earthquakes: Consequences for Physical Models”. In: *Bulletin of the Seismological Society of America* 72.1, pp. 1–14. ISSN: 0037-1106. DOI: 10.1785/BSSA0720010001.
- Scholz, Christopher H. and Juan C. Contreras (1998). “Mechanics of Continental Rift Architecture”. In: *Geology* 26.11, pp. 967–970. ISSN: 0091-7613. DOI: 10.1130/0091-7613(1998)026<0967:MOCRA>2.3.CO;2.
- Sibson, Richard H. (2004). “Controls on Maximum Fluid Overpressure Defining Conditions for Mesozonal Mineralisation”. en. In: *Journal of Structural Geology* 26.6, pp. 1127–1136. ISSN: 0191-8141. DOI: 10.1016/j.jsg.2003.11.003.
- Siebert, L, T Simkin, and P Kimberly (2011). *Volcanoes of the World*. University of California Press.
- Sloan, R. A. and J. A. Jackson (2012). “Upper-Mantle Earthquakes beneath the Arafura Sea and South Aru Trough: Implications for Continental Rheology”. en. In: *Journal of Geophysical Research: Solid Earth* 117.B5. ISSN: 2156-2202. DOI: 10.1029/2011JB008992.
- Sloan, R. A., J. A. Jackson, D. McKenzie, and K. Priestley (2011). “Earthquake Depth Distributions in Central Asia, and Their Relations with Lithosphere Thickness, Shortening and Extension: Earthquake Depth Distributions in Central Asia”. en. In: *Geophysical Journal International* 185.1, pp. 1–29. ISSN: 0956540X. DOI: 10.1111/j.1365-246X.2010.04882.x.
- Spakman, Wim and Robert Hall (2010). “Surface Deformation and Slab–Mantle Interaction during Banda Arc Subduction Rollback”. en. In: *Nature Geoscience* 3.8, pp. 562–566. ISSN: 1752-0894, 1752-0908. DOI: 10.1038/ngeo917.
- Stevens, Colleen W., Robert Mccaffrey, Yehuda Bock, Joachim F. Genrich, Manuel Pubellier, and Cecep Subarya (2002). “Evidence for Block Rotations and Basal Shear in the World’s Fastest

- Slipping Continental Shear Zone in Nw New Guinea”. en. In: *Geodynamics Series*. Ed. by Seth Stein and Jeffrey T. Freymueller. Washington, D. C.: American Geophysical Union, pp. 87–99. ISBN: 978-1-118-67044-6 978-0-87590-532-7. DOI: 10.1029/GD030p0087.
- Taymaz, T., J. Jackson, and R. Westaway (1990). “Earthquake Mechanisms in the Hellenic Trench near Crete”. en. In: *Geophysical Journal International* 102.3, pp. 695–731. ISSN: 0956540X, 1365246X. DOI: 10.1111/j.1365-246X.1990.tb04590.x.
- Teas, Philip A., John Decker, Dan Orange, and Peter Baillie (2009). “New Insight Into Structure and Tectonics of the Seram Trough From SeaSeep™ High Resolution Bathymetry”. en-US. In: Townend, John and Mark D Zoback (2000). “How Faulting Keeps the Crust Strong”. en. In: p. 4.
- Tregoning, P. and A. Gorbatov (2004). “Evidence for Active Subduction at the New Guinea Trench”. en. In: *Geophysical Research Letters* 31.13. ISSN: 1944-8007. DOI: 10.1029/2004GL020190.
- Turcotte, Donald L. and Gerald Schubert (2002). *Geodynamics*. en. Cambridge University Press. ISBN: 978-0-521-66624-4.
- Veevers, J. J. (2000). *Billion-Year Earth History of Australia and Neighbours in Gondwanaland*. en. GEMOC Press. ISBN: 978-1-876315-04-7.
- Veevers, J.J., C.McA. Powell, and S.R. Roots (1991). “Review of Seafloor Spreading around Australia. I. Synthesis of the Patterns of Spreading”. en. In: *Australian Journal of Earth Sciences* 38.4, pp. 373–389. ISSN: 0812-0099, 1440-0952. DOI: 10.1080/08120099108727979.
- Visser, W and J Hermes (1962). “Geological Results of the Exploration for Oil in Netherlands New Guinea”. In: *Government Printing Office, The Hague*, p. 256.
- Wallace, Laura M., Colleen Stevens, Eli Silver, Rob McCaffrey, Wesley Loratung, Suvenia Hasiata, Richard Stanaway, Robert Curley, Robert Rosa, and Jones Taugaloidi (2004). “GPS and Seismological Constraints on Active Tectonics and Arc-Continent Collision in Papua New Guinea: Implications for Mechanics of Microplate Rotations in a Plate Boundary Zone”. en. In: *Journal of Geophysical Research: Solid Earth* 109.B5. ISSN: 2156-2202. DOI: 10.1029/2003JB002481.
- Webb, Laura E., Suzanne L. Baldwin, and Paul G. Fitzgerald (2014). “The Early-Middle Miocene Subduction Complex of the Louisiade Archipelago, Southern Margin of the Woodlark Rift”. en. In: *Geochemistry, Geophysics, Geosystems* 15.10, pp. 4024–4046. ISSN: 1525-2027. DOI: 10.1002/2014GC005500.
- Weissel, Jeffrey K. and A. B. Watts (1979). “Tectonic Evolution of the Coral Sea Basin”. en. In: *Journal of Geophysical Research: Solid Earth* 84.B9, pp. 4572–4582. ISSN: 2156-2202. DOI: 10.1029/JB084iB09p04572.
- Weller, Owen M., Simon Jackson, William G. R. Miller, Marc R. St-Onge, and Nicole Rayner (2020). “Quantitative Elemental Mapping of Granulite-Facies Monazite: Textural Insights and Implications for Petrochronology”. en. In: *Journal of Metamorphic Geology* 38.8, pp. 853–880. ISSN: 1525-1314. DOI: 10.1111/jmg.12552.

- Wessel, P., J. F. Luis, L. Uieda, R. Scharroo, F. Wobbe, W. H. F. Smith, and D. Tian (2019). “The Generic Mapping Tools Version 6”. en. In: *Geochemistry, Geophysics, Geosystems* 20.11, pp. 5556–5564. ISSN: 1525-2027. DOI: 10.1029/2019GC008515.
- Weston, J., E. R. Engdahl, J. Harris, D. Di Giacomo, and D. A. Storchak (2018). “ISC-EHB: Reconstruction of a Robust Earthquake Data Set”. en. In: *Geophys J Int* 214.1, pp. 474–484. ISSN: 0956-540X. DOI: 10.1093/gji/ggy155.
- White, L. T., R. Hall, I. Gunawan, and B. Kohn (2019). “Tectonic Mode Switches Recorded at the Northern Edge of the Australian Plate During the Pliocene and Pleistocene”. en. In: *Tectonics* 38.1, pp. 281–306. ISSN: 1944-9194. DOI: 10.1029/2018TC005177.
- Whittington, Alan G., Anne M. Hofmeister, and Peter I. Nabelek (2009). “Temperature-Dependent Thermal Diffusivity of the Earth’s Crust and Implications for Magmatism”. en. In: *Nature* 458.7236, pp. 319–321. ISSN: 1476-4687. DOI: 10.1038/nature07818.
- Wimpenny, Sam, Alex Copley, Carlos Benavente, and Enoch Aguirre (2018). “Extension and Dynamics of the Andes Inferred From the 2016 Parina (Huarichancara) Earthquake”. en. In: *Journal of Geophysical Research: Solid Earth* 123.9, pp. 8198–8228. ISSN: 2169-9356. DOI: 10.1029/2018JB015588.
- Yakymchuk, Chris and Michael Brown (2019). “Divergent Behaviour of Th and U during Anatexis: Implications for the Thermal Evolution of Orogenic Crust”. en. In: *Journal of Metamorphic Geology* 37.7, pp. 899–916. ISSN: 1525-1314. DOI: 10.1111/jmg.12469.
- Zwick, P., R. McCaffrey, and G. Abers (1994). “MT5 Program”. In: *IASPEI Software Library*.

Tables and Figures

Table 1: Earthquake source parameters determined in this study using body-waveform modelling. Locations are taken from the NEIC catalogue. Depths and focal mechanisms have been determined using the MT5 program, except for the events marked † for which focal mechanisms could not be accurately obtained. For these two events, the gCMT focal mechanism has been retained (Dziewonski et al., 1981; Ekström et al., 2012), and only depth, source time function, and seismic moment inverted for.

| Body-waveform modelling | | | | | | | | | | | | |
|-------------------------|----|----|------|----|----|--------|-------|-------|-------|-----------------|---------|----------|
| Date | | | Time | | | Long | Lat | M_w | Depth | Focal mechanism | | |
| yyyy | mm | dd | hh | mm | ss | (°) | (°) | | (km) | Strike (°) | Dip (°) | Rake (°) |
| 1992 | 05 | 25 | 02 | 51 | 32 | 139.73 | -4.79 | 5.7 | 6 | 303 | 66 | 22 |
| 1993 | 06 | 12 | 18 | 26 | 42 | 135.12 | -4.38 | 6 | 10 | 251 | 72 | 19 |
| 1994 | 01 | 04 | 19 | 31 | 59 | 135.15 | -4.30 | 6 | 8 | 69 | 86 | 350 |
| 1995 | 03 | 13 | 10 | 31 | 46 | 134.38 | -2.79 | 5.8 | 7 | 208 | 58 | 272 |
| 2000 | 03 | 03 | 22 | 22 | 40 | 143.81 | -6.82 | 6.6 | 18 | 122 | 52 | 82 |
| †2005 | 02 | 02 | 06 | 28 | 36 | 145.04 | -7.48 | 5.5 | 14 | 63 | 59 | 68 |
| 2007 | 08 | 20 | 21 | 30 | 45 | 140.87 | -5.40 | 5.7 | 11 | 149 | 34 | 91 |
| 2011 | 11 | 15 | 23 | 42 | 29 | 140.31 | -5.28 | 5.7 | 14 | 126 | 48 | 52 |
| 2012 | 10 | 12 | 00 | 31 | 28 | 134.03 | -4.89 | 6.6 | 23 | 183 | 54 | 243 |
| 2012 | 12 | 08 | 16 | 35 | 16 | 143.97 | -7.21 | 5.8 | 9 | 133 | 54 | 99 |
| †2013 | 09 | 05 | 15 | 27 | 03 | 144.03 | -7.27 | 5.4 | 5 | 112 | 54 | 85 |
| 2014 | 07 | 28 | 23 | 0 | 48 | 143.87 | -6.92 | 5.6 | 13 | 131 | 44 | 100 |
| 2018 | 03 | 06 | 14 | 13 | 07 | 142.61 | -6.30 | 6.7 | 10 | 135 | 75 | 93 |
| 2019 | 01 | 26 | 08 | 12 | 48 | 133.77 | -5.50 | 5.9 | 30 | 204 | 58 | 253 |

Table 2: Earthquake depths determined using depth-phase analysis in this study. Locations are taken from the NEIC catalogue. Focal mechanisms and moment have been retained from the gCMT catalogue (Dziewonski et al., 1981; Ekström et al., 2012).

| Date | | Time | | Depth-phase analysis | | | | | | gCMT mechanism | | |
|------|----|------|----|----------------------|----|-------------|------------|-------|---------------|----------------|---------|----------|
| yyyy | mm | dd | hh | mm | ss | Long (°) | Lat (°) | M_w | Depth (km) | Strike (°) | Dip (°) | Rake (°) |
| 1991 | 02 | 23 | 19 | 53 | 16 | 137.71 | -4.68 | 5.2 | 6 | 108 | 64 | 99 |
| 1995 | 01 | 21 | 16 | 44 | 07 | 134.35 | -2.60 | 5.2 | 7 | 214 | 58 | 292 |
| 1999 | 10 | 25 | 00 | 43 | 06 | 134.19 | -2.12 | 5.4 | 8 | 31 | 38 | 267 |
| 2001 | 07 | 12 | 19 | 37 | 15 | 134.84 | -3.65 | 5.1 | 8 | 191 | 60 | 251 |
| 2002 | 09 | 28 | 15 | 14 | 57 | 134.57 | -3.26 | 5 | 10 | 26 | 55 | 283 |
| 2007 | 08 | 19 | 19 | 09 | 45 | 140.85 | -5.37 | 5.3 | 9 | 80 | 87 | 3 |
| 2009 | 10 | 29 | 01 | 34 | 00 | 140.38 | -5.26 | 5.1 | 19 | 140 | 43 | 101 |
| 2016 | 06 | 14 | 22 | 09 | 28 | 137.97 | -4.60 | 5.2 | 33 | 296 | 68 | 129 |
| 2019 | 04 | 27 | 13 | 32 | 53 | 137.23 | -4.32 | 4.9 | 8 | 235 | 26 | 293 |

Table 3: Parameters used to calculate the horizontal force exerted between the New Guinea Highlands and forelands, and to estimate the frictional strength of crustal faults in the foreland basin. The parameters taken from Karato and Wu (1993) are for a dry olivine dislocation creep law: $\Delta\sigma_{xx} = S\dot{\epsilon}_r^{\frac{1}{n}} A^{\frac{-1}{n}} \exp(\frac{E+PV}{nRT})$, where $\Delta\sigma_{xx}$ is the differential stress, S is the shear modulus, $\dot{\epsilon}$ is the reference strain rate, A is a constant, n is the power law exponent, E is the activation energy, P is pressure, V is the activation volume, R is the gas constant, and T is temperature.

| Variable | Value | | Source |
|---|---|-------------|--|
| | West | East | |
| Crustal thickness (lowlands) | 30–35 km | 30–35 km | Jacobson et al. (1979); Clitheroe et al. (2000) |
| Crustal thickness (mountains) | 40–60 km | 40–60 km | Abers and McCaffrey (1988); Abers and Roecker (1991) |
| Lithosphere thickness (lowlands) | 100–150 km | 50–100 km | Priestley et al. (2018) |
| Lithosphere thickness (mountains) | 100–160 km | 50–110 km | Priestley et al. (2018) |
| Moho temperature (lowlands) | 400–600°C | 550–800°C | This study |
| Moho temperature (mountains) | 500–800°C | 600–1000°C | This study |
| Foreland seismogenic thickness | 33–36 km | 20–27 km | This study |
| Foreland sediment thickness | 1.5–5 km | 0.1–1.5 km | Visser and Hermes (1962) |
| Foreland fault dips | 27–87° | 15–75° | This study |
| Relief | 2–3 km | 1.5–2.75 km | This study |
| Mantle potential temperature | 1315°C | | McKenzie et al. (2005) |
| Thermal expansivity of crust | $3 \times 10^{-5} \text{ K}^{-1}$ | | Turcotte and Schubert (2002) |
| Thermal expansivity of mantle | $3\text{--}4.5 \times 10^{-5} \text{ K}^{-1}$ | | Bouhfid et al. (1996) |
| Asthenosphere density (ρ_a , 0°C) | 3300 kg/m ³ | | Turcotte and Schubert (2002) |
| Lithosphere mantle density (0°C) | $\rho_a - 60 \text{ kg/m}^3$ | | Turcotte and Schubert (2002) |
| Crustal density | 2800 kg/m ³ | | Turcotte and Schubert (2002) |
| Pre-exponential factor (A) | $3.5 \times 10^{22} \text{ s}^{-1}$ | | Karato and Wu (1993) |
| Activation energy (E) | 540 kJ/mol | | Karato and Wu (1993) |
| Activation volume (V) | 20 cm ³ /mol | | Karato and Wu (1993) |
| Stress exponent (n) | 3.5 | | Karato and Wu (1993) |

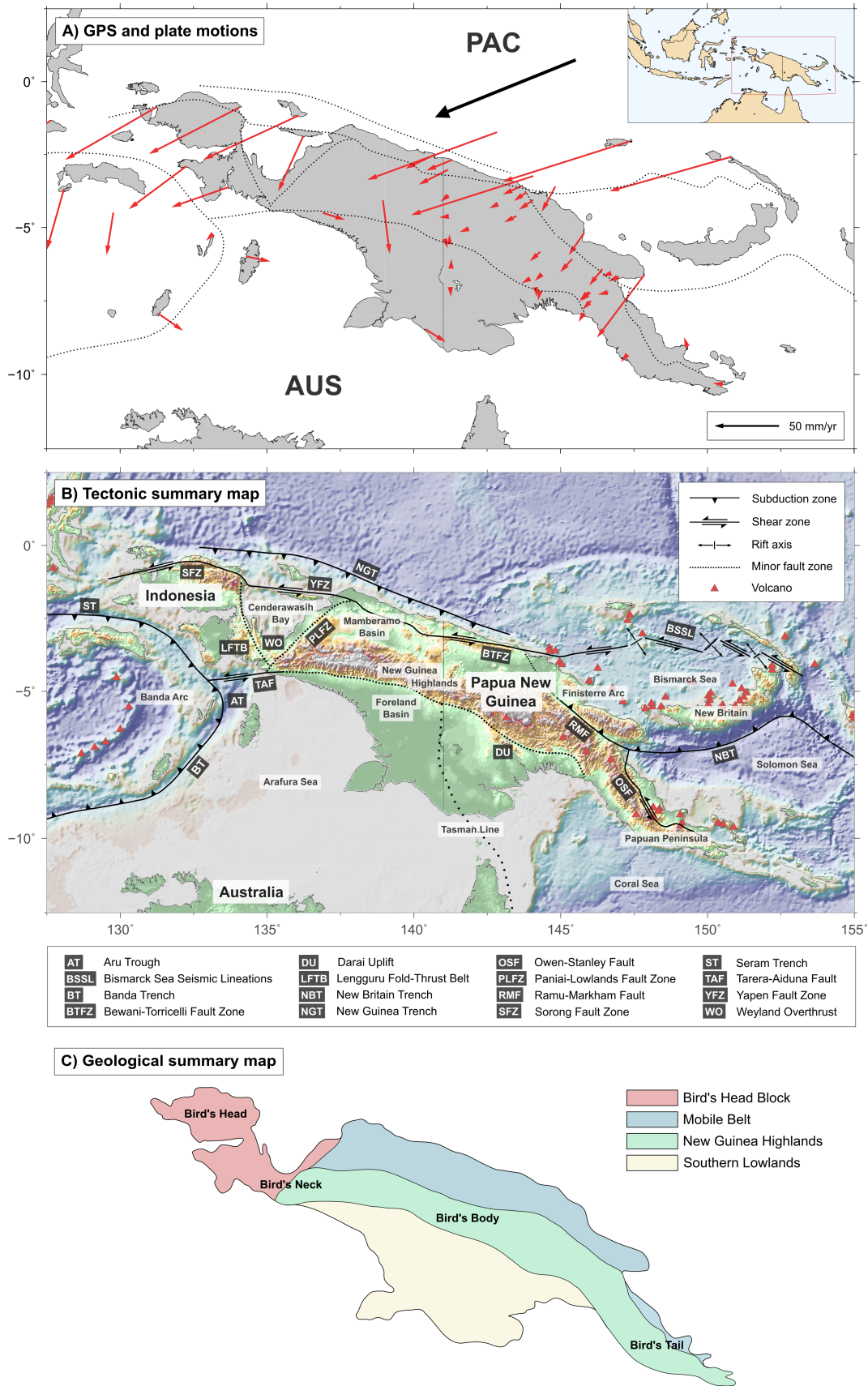


Figure 1: (Caption on following page)

Figure 1: **A:** GPS data (red arrows) showing motion relative to Australian Plate (AUS). GPS data west of 141°E are from Stevens et al. (2002); GPS data east of 141°E are from Koulali et al. (2015). The large black arrow indicates motion of the Pacific Plate (PAC) relative to the Australian Plate (DeMets et al., 1994). Dotted lines indicate key fault zones adapted from Baldwin et al. (2012). **B:** Tectonic summary map of New Guinea showing major geological features and fault zones, adapted from Baldwin et al. (2012). Red triangles indicate locations of known volcanoes (Siebert et al., 2011). Acronyms of the names of fault zones are listed below the map. **C:** Simplified geological map of New Guinea adapted from Hill and Hall (2003) and Baldwin et al. (2012).

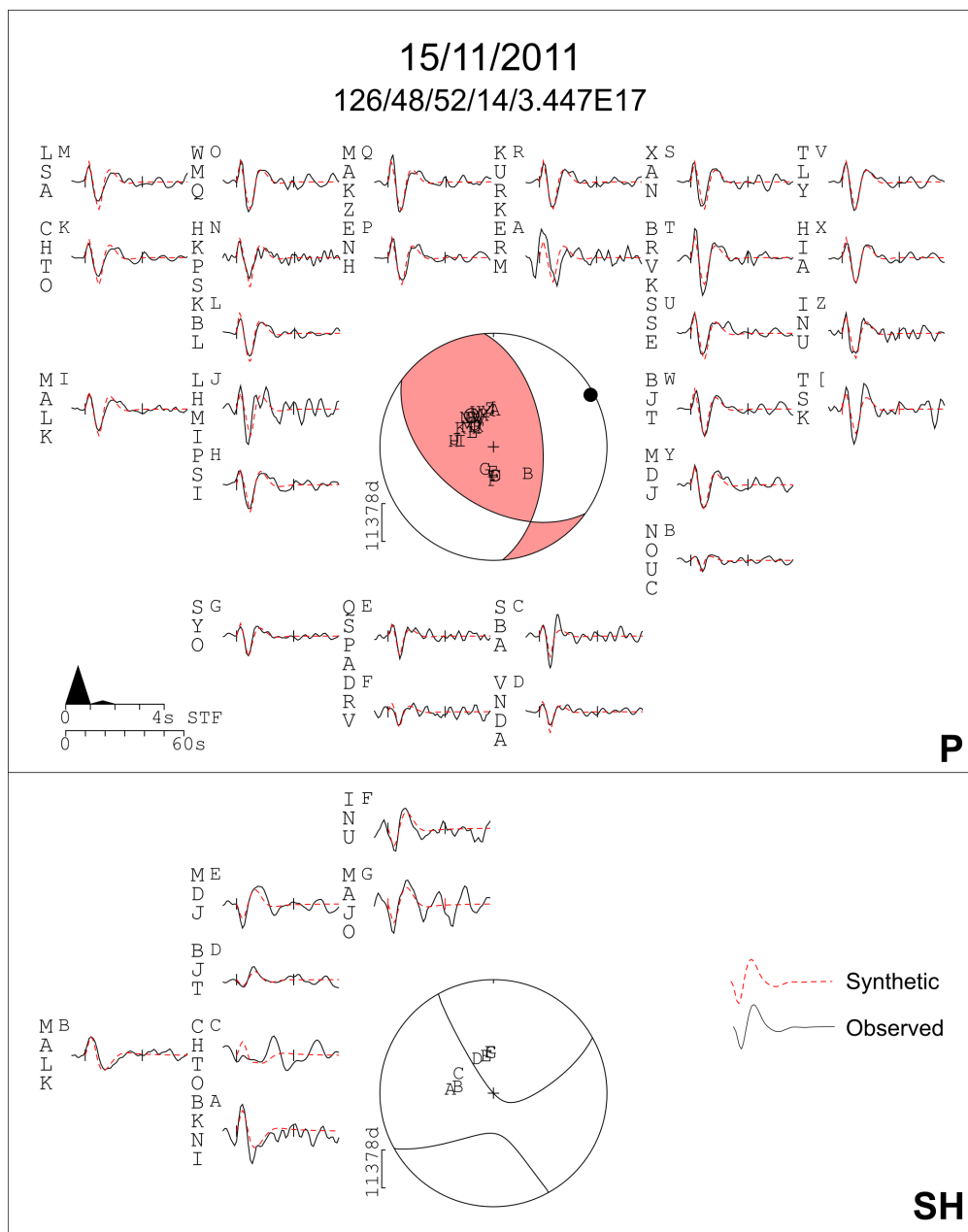


Figure 2: Minimum-misfit focal mechanism solution for the 15th November 2011 M_w 5.7 earthquake in the New Guinea forelands, determined using teleseismic body-waveform modelling in the MT5 program. Source parameters from the inversion are shown beneath the title in the form: strike/dip/rake/centroid depth/seismic moment, where centroid depth is in kilometres and seismic moment is in newton metres. The upper panel shows the lower-hemisphere stereographic projection of the P-waveform nodal planes and the locations of seismic stations used in the inversion. The lower panel shows the SH-waveform equivalent. Letters printed on the focal spheres correspond to letters next to the seismic station codes, ordered by azimuthal location. Seismic station codes are printed to the left of each seismogram. Black and white circles on the focal spheres represent the projections of the P and T axes respectively. The black lines and dashed red lines represent the observed and synthetic seismograms, respectively. Vertical ticks on each seismogram mark the inversion window. STF represents the best-fit source-time function, with the timescale for the inverted waveforms shown directly below.

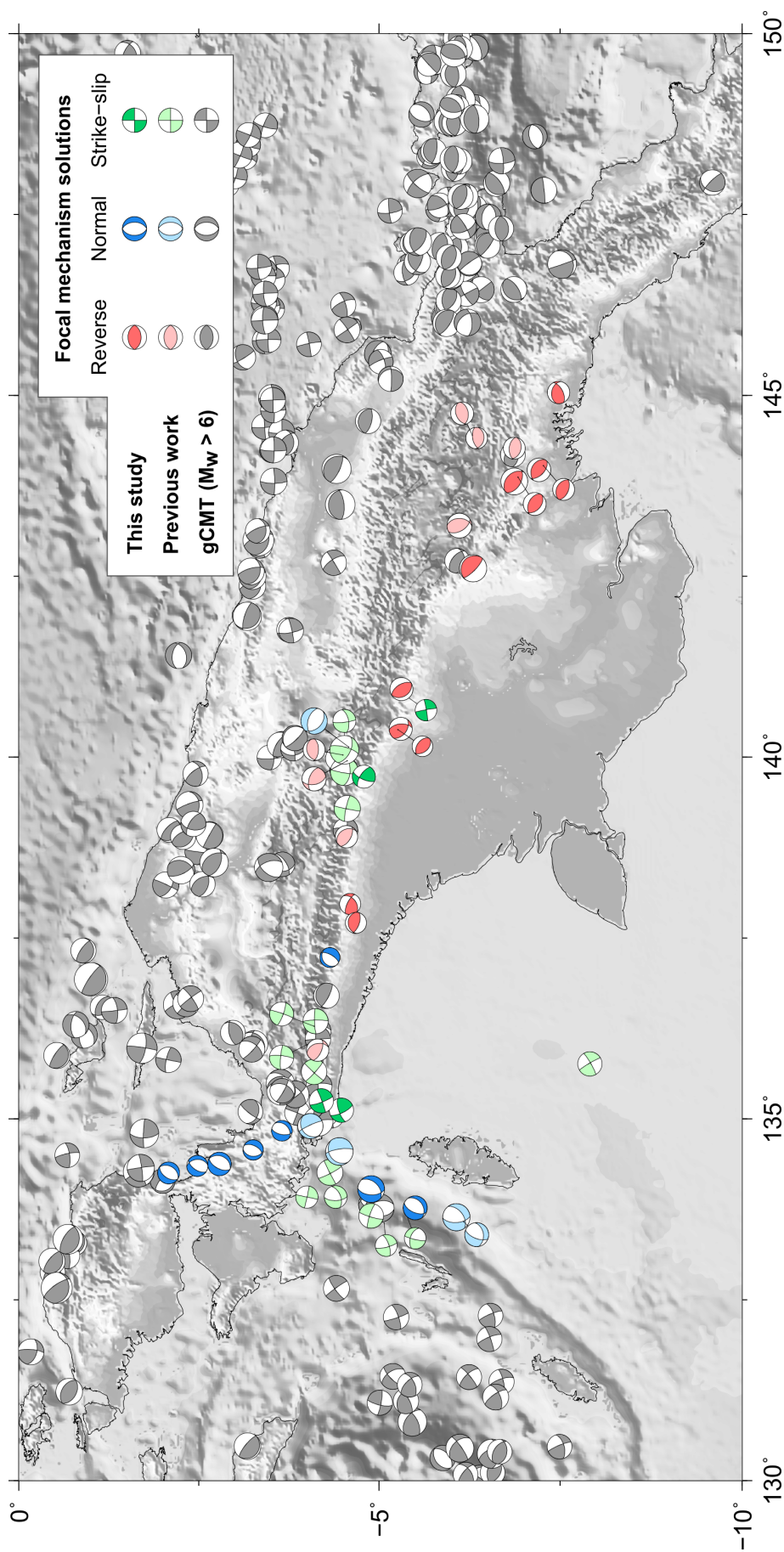


Figure 3: Focal mechanism solutions determined by body-waveform modelling or depth-phase analysis in this study, or by body-waveform modelling in previous work (Abers and McCaffrey, 1988; Sloan and Jackson, 2012). Additional events of $M_w > 6$ are taken from the gCMT catalogue (Dziewonski et al., 1981; Ekström et al., 2012).

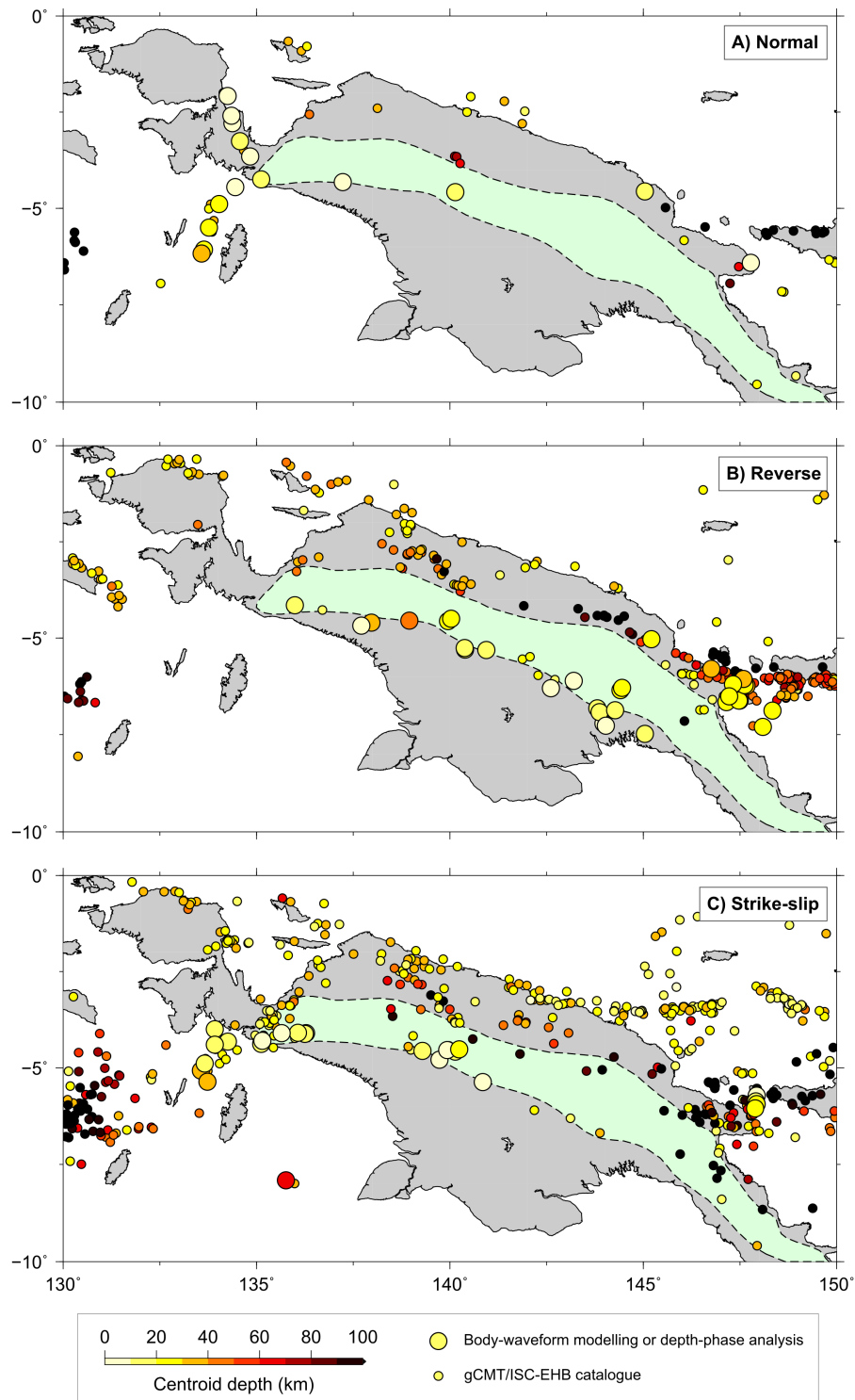


Figure 4: Maps of earthquake locations and depths, separated by focal mechanism. Large circles represent results from body-waveform modelling or depth-phase analysis in this study and previous work (Abers and McCaffrey, 1988; McCaffrey and Abers, 1991; Sloan and Jackson, 2012). Additional events of $M_w \geq 5.5$ are shown as small circles and are taken from a catalogue of gCMT focal mechanism solutions combined with depths from the ISC-EHB Bulletin (Dziewonski et al., 1981; Ekström et al., 2012; International Seismological Centre, 2020). The green outline marks the extent of the New Guinea Highlands.

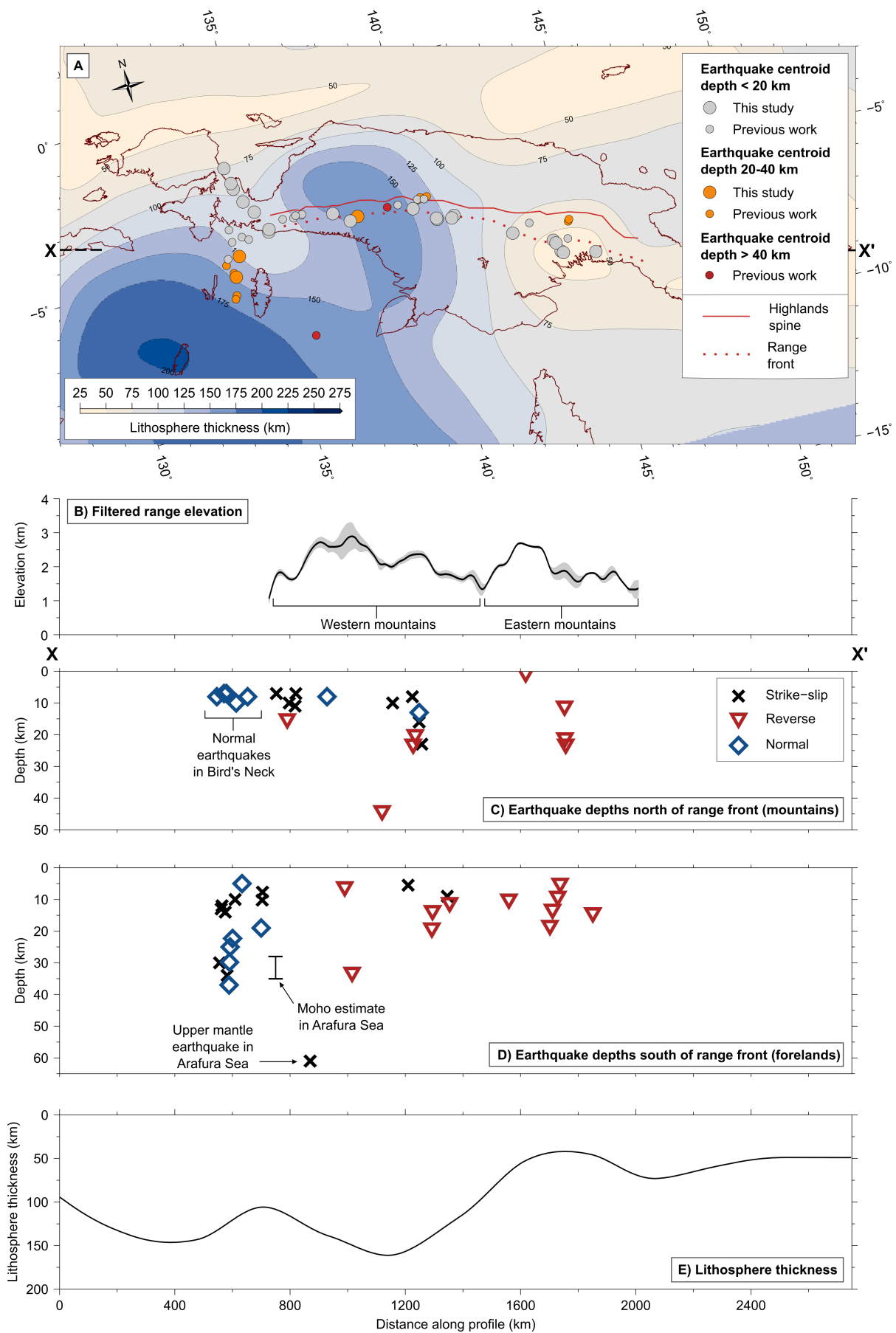


Figure 5: (Caption on following page)

Figure 5: **A:** Earthquake depths determined by body-waveform modelling or depth-phase analysis in this study or by previous work (Abers and McCaffrey, 1988; Sloan and Jackson, 2012), shown on a map of lithosphere thickness (Priestley et al., 2018). The lower bound on horizontal resolution of the lithosphere thickness data is ~ 250 km, and the vertical resolution is ~ 30 km. The lithosphere thickness data were defined on a 2-degree grid and have been interpolated to show a smoothed data set. Earthquakes are coloured according to centroid depth. X and X' represent the end points of the cross-section used in the lower panels. The solid red line represents the topographic spine of the New Guinea Highlands and the dotted red line represents the range front. **B:** Topography of the New Guinea Highlands was taken from a 50 km swath along the spine of the New Guinea Highlands, from a 100 km Gaussian filtered version of the ETOPO2 dataset. The black line represents mean elevation and the grey outline represents the standard deviation. **C and D:** Centroid depths of earthquakes from Panel A have been projected onto a vertical cross-section along-strike of the mountains, separated by whether the earthquake occurs north of the range front (within the mountains) or south of the range front (within the foreland basin or Arafura Sea). Estimates of Moho depth from the Arafura Sea (Jacobson et al., 1979) are taken to represent the crustal thickness of the northern Australian Shield. **E:** Lithosphere thickness plotted along the cross-section X-X'.

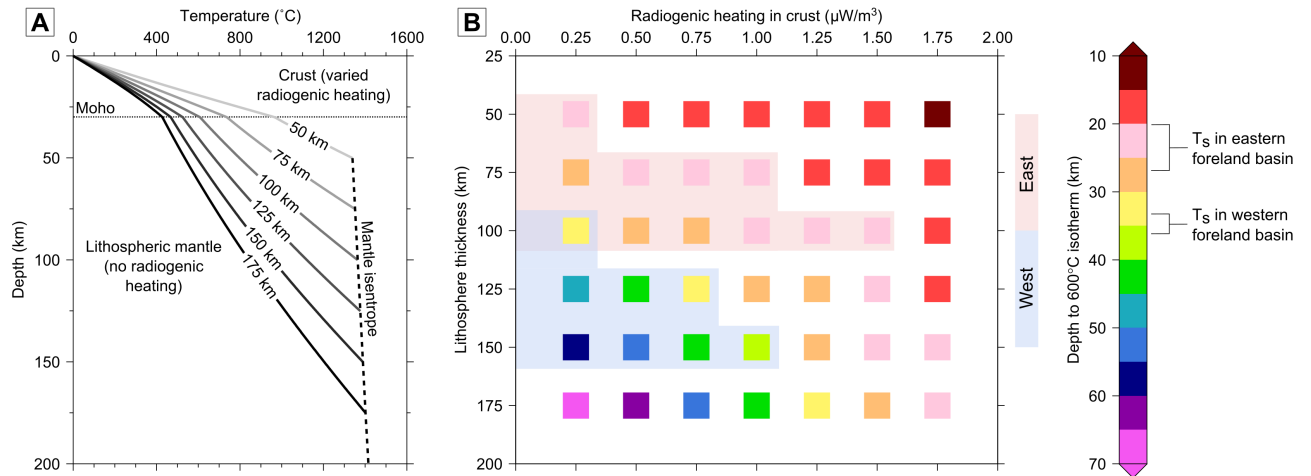


Figure 6: **A:** Steady-state geotherms calculated for different values of lithosphere thickness, as indicated. These geotherms were calculated using a crustal thickness of 30 km and constant radiogenic heating in the crust of $0.50 \mu\text{W}/\text{m}^3$, but the radiogenic heating was varied in other models not shown on this plot. **B:** Depth to the 600°C isotherm plotted as a function of lithosphere thickness and radiogenic heating in the crust. The blue region represents the parameter space for the western foreland basin over which the depth to the 600°C isotherm is greater than or equal to the observed seismogenic thickness (T_s) and the lithosphere thickness is consistent with the results of Priestley et al. (2018). The pink region represents the corresponding parameter space for the eastern foreland basin.

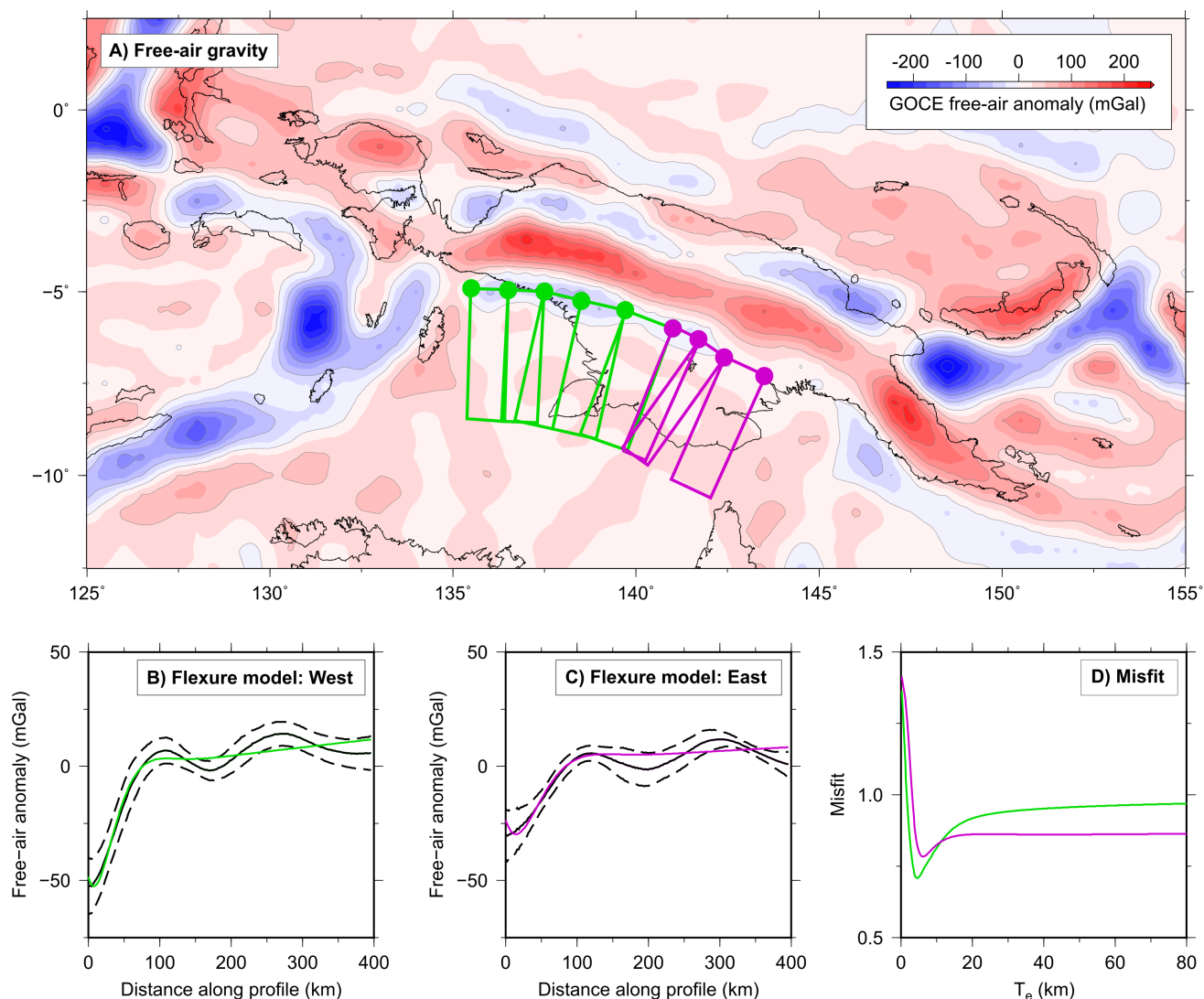


Figure 7: **A:** GOCE free-air gravity map of New Guinea (Drinkwater et al., 2007). The green and purple coloured boxes represent the region over which profiles through the gravity field, perpendicular to the range front, have been stacked along the length of the west and east foreland basin respectively. The coloured circles represent nodes which have been placed over the gravity minimum. **B and C:** Mean (solid black line) and standard deviation bounds (dashed black lines) for the stacked GOCE free-air gravity anomalies, and the best-fitting flexural model to the observed gravity profile (solid coloured line). **D:** Weighted misfit between the observed and modelled gravity field, plotted as a function of elastic thickness of the underthrusting Australian Plate. The best-fitting solutions for the west and east occur at $T_e = 4.6$ km and $T_e = 6.2$ km respectively.

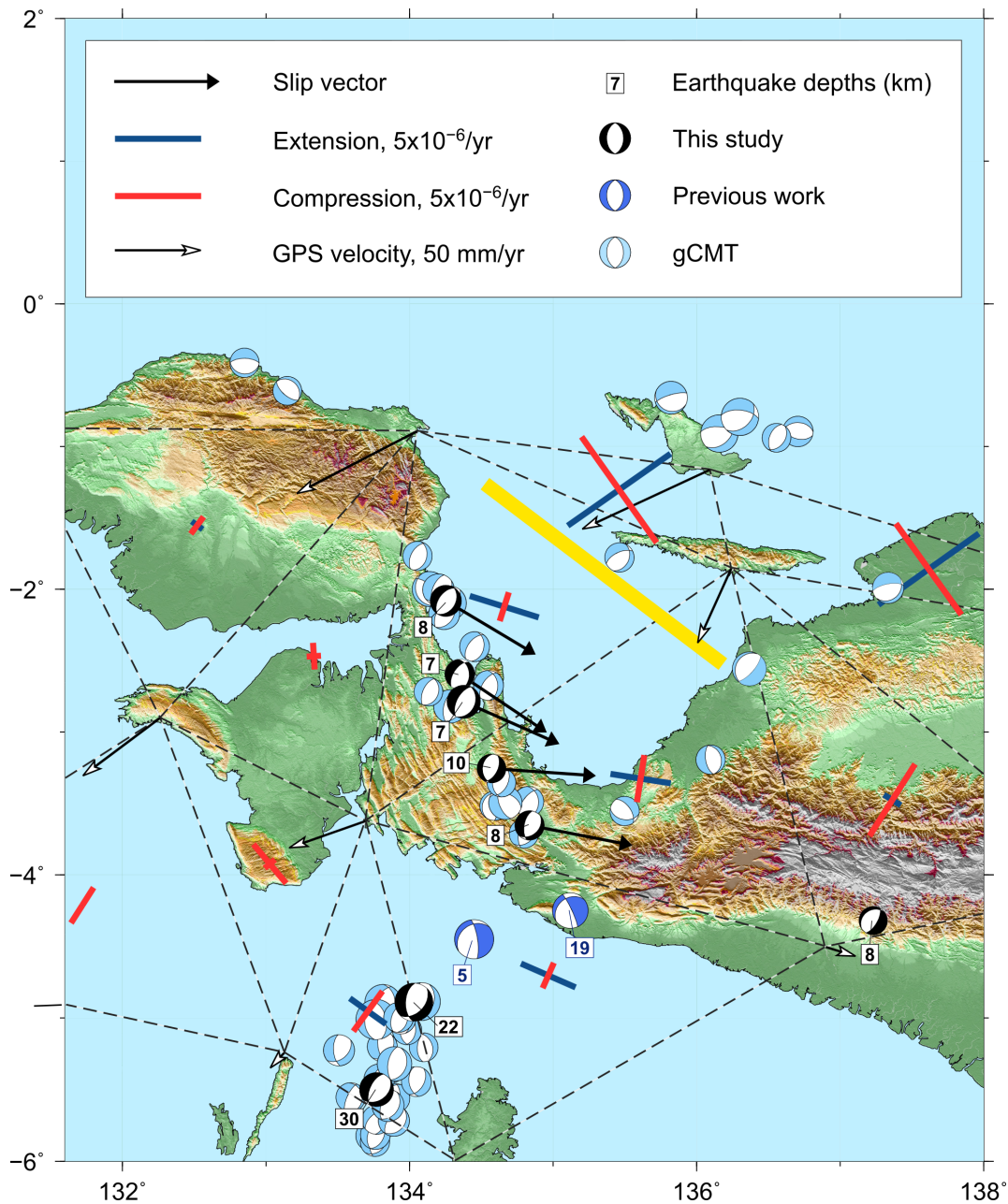


Figure 8: SRTM 30 m DEM overlain with a summary of normal faulting in western New Guinea, showing focal mechanisms, depths, and selected slip vectors of earthquakes determined using body-waveform modelling or depth-phase analysis in this study or previous work (McCaffrey and Abers, 1988; Sloan and Jackson, 2012). Additional focal mechanisms for normal earthquakes are taken from the gCMT catalogue (Dziewonski et al., 1981; Ekström et al., 2012). GPS velocities are shown relative to the Australian Plate (Stevens et al., 2002). Grey dashed lines delineate the triangulated network of GPS stations from which strain rates were calculated. The yellow line shows the location of the seismic reflection profile shown in Figure 10.

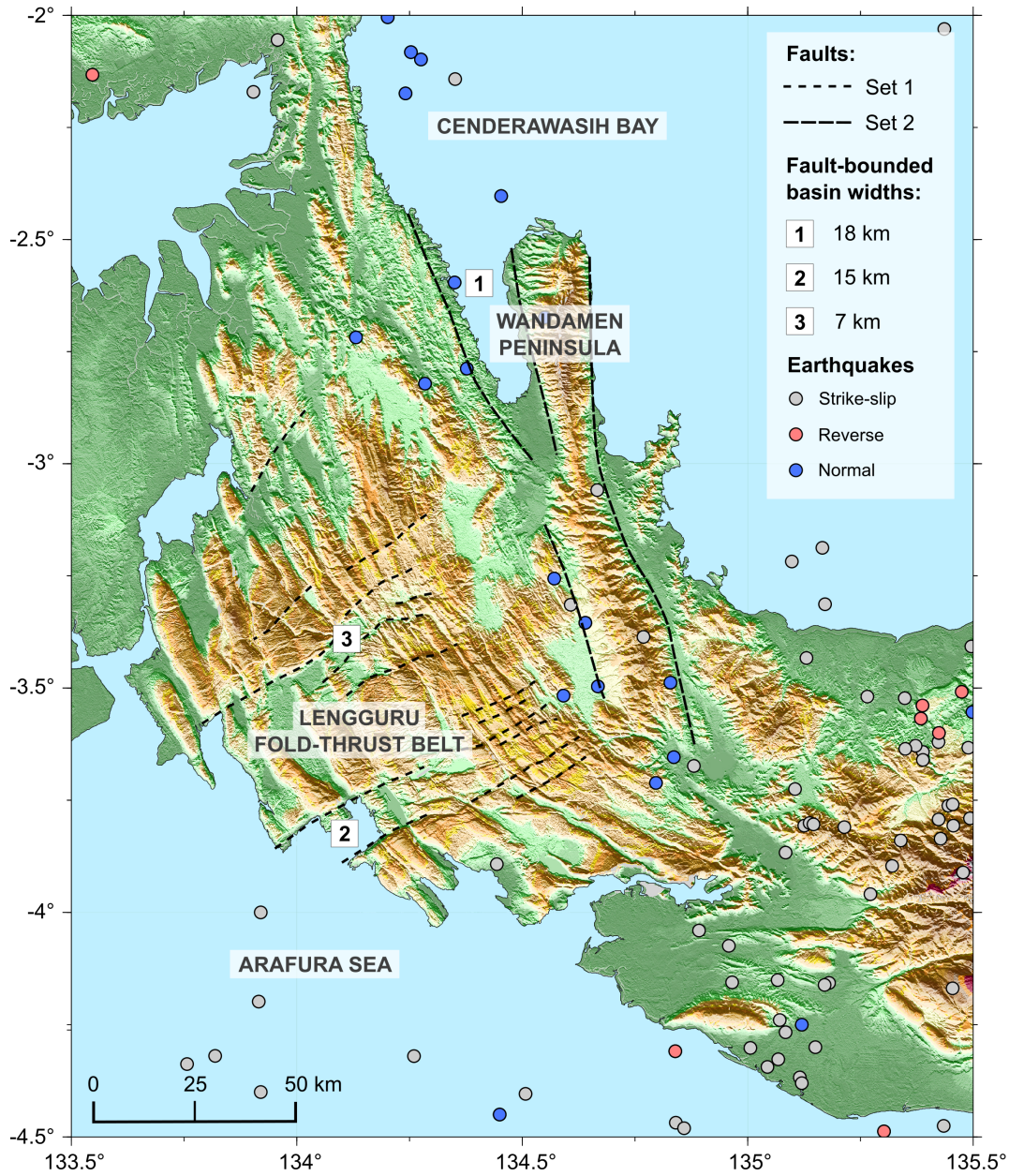


Figure 9: SRTM 30 m DEM of the Bird's Neck region. Normal faults are shown as dashed black lines. The width of fault-bounded basins are also indicated. Earthquake hypocenters from the gCMT catalogue are coloured according to focal mechanism.

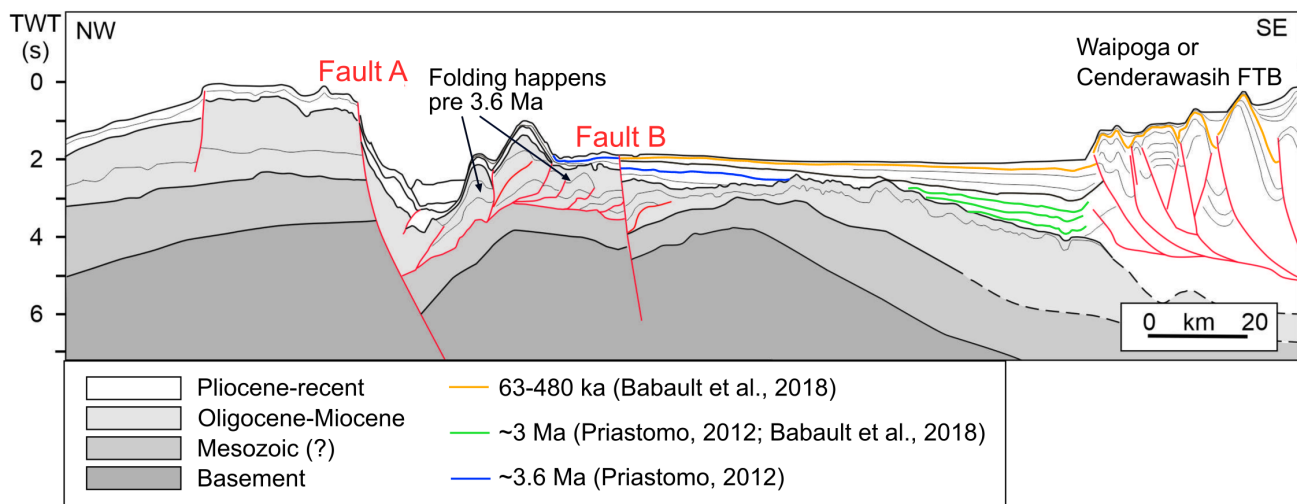


Figure 10: Interpretation of 2D seismic reflection profile CE07-17 across Cenderawasih Bay, modified after Priastomo (2012). The location of the seismic line is shown in Figure 8. The age of the horizons is from Priastomo (2012) and Babault et al. (2018). Decker et al. (2009) and Sapiie et al. (2010) interpreted the lower sequence as syn- and post-rift passive margin sediments (mid and light grey units in the figure) overlying a basement (darker grey). Slip on fault B happens post 3.6 My. In the Waipoga Fold-and-Thrust Belt, the base of the syn-tectonic sediments is dated at ~63–480 ka (Babault et al., 2018).

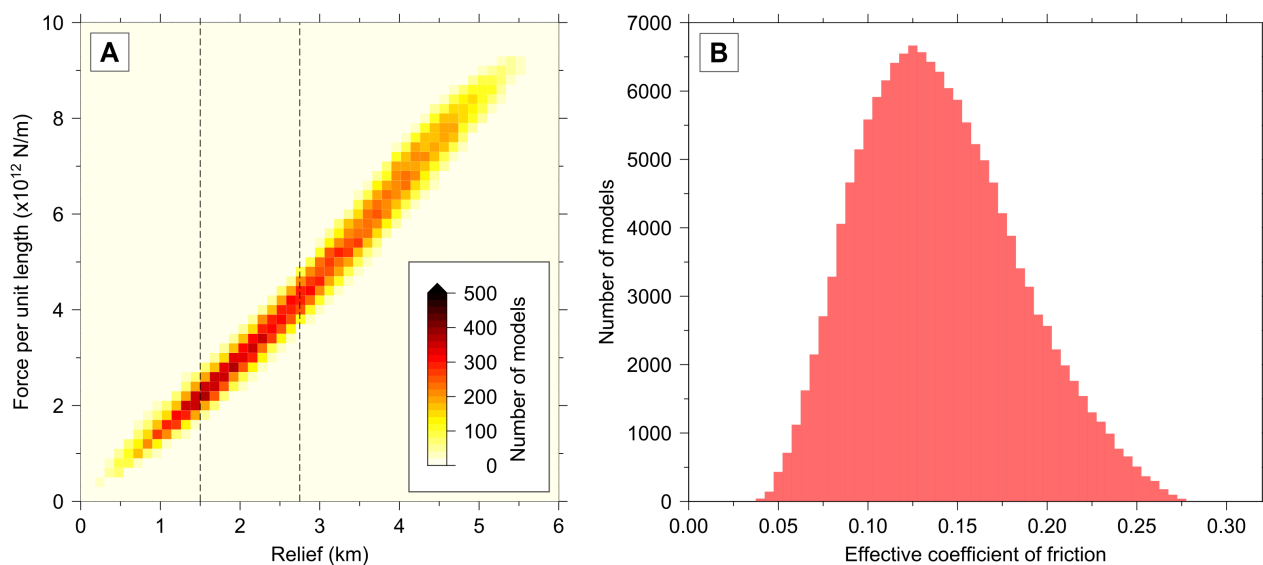


Figure 11: **A:** Results of calculations for force per unit length transmitted through the lithosphere due to gravitational potential energy differences between the eastern New Guinea Highlands and forelands. The transmitted force was calculated by varying lithosphere thickness, crustal thickness, and temperature structure. Force per unit length is shown as a function of relief between the mountains and lowlands. The vertical black dashed lines represent the range of appropriate solutions given the range of relief observed in the eastern New Guinea Highlands. **B:** Estimates of the effective coefficient of friction on crustal faults in the east foreland basin. Calculations have assumed the entire crust is in compression and that the lithosphere mantle deforms via dislocation creep at temperatures above 600°C .

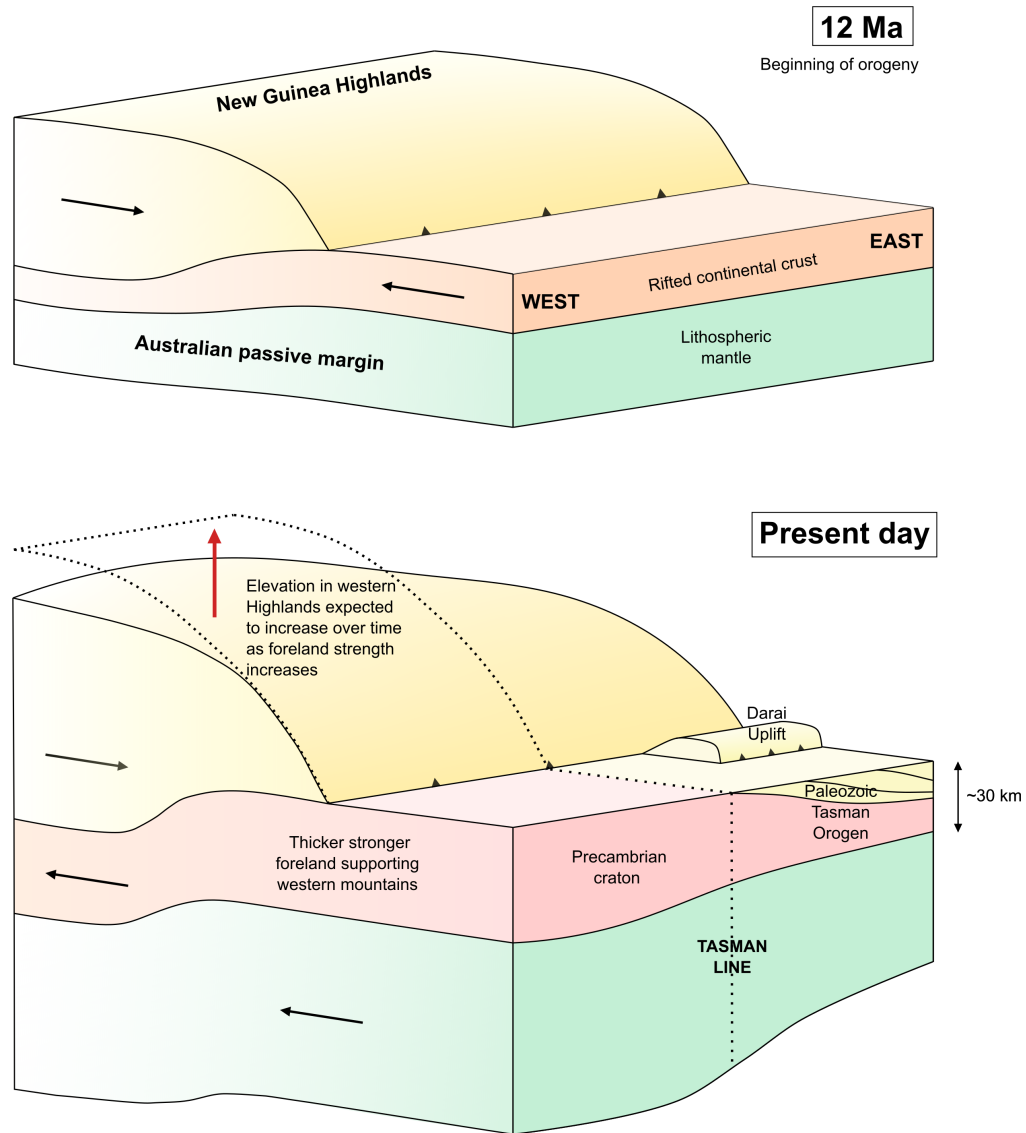


Figure 12: Schematic diagram of the New Guinea Highlands showing how the lithosphere and mountain elevation has evolved since the beginning of the orogeny, and how it may be expected to evolve over time due to changes in the rheology of the underthrusting Australian Plate.

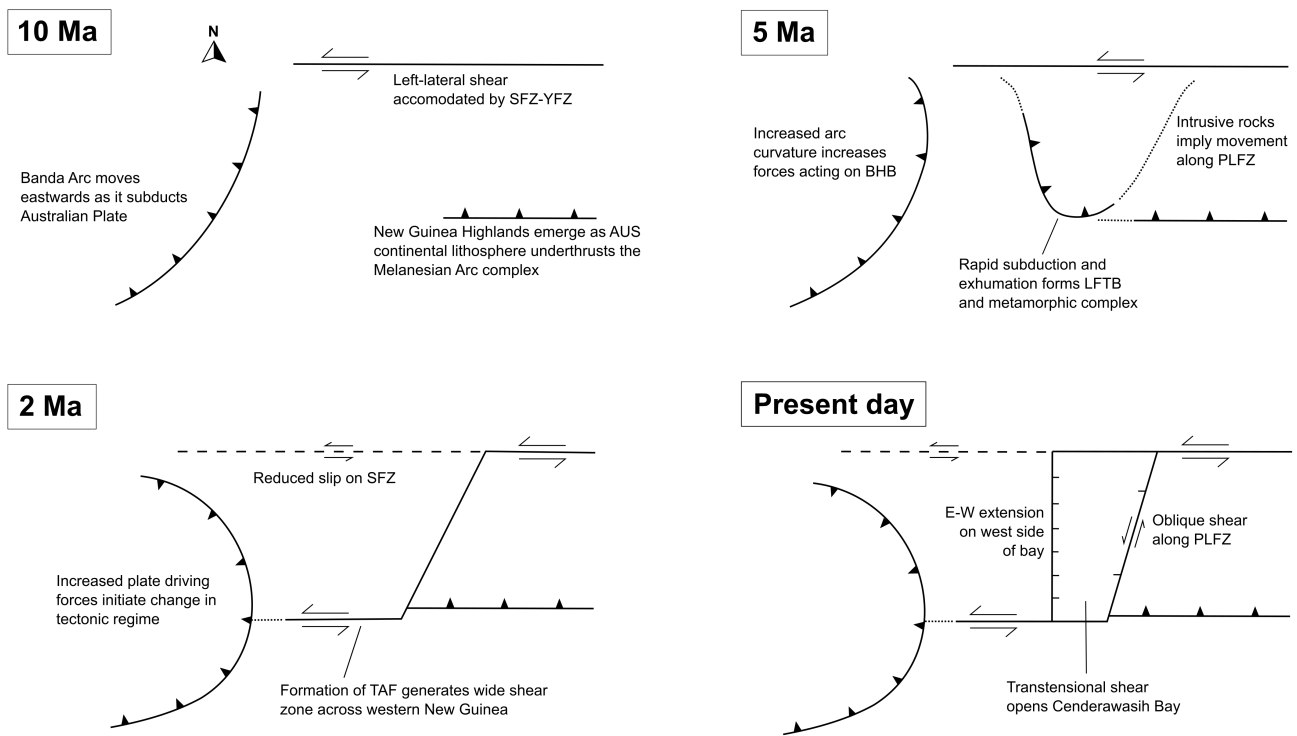


Figure 13: A simplified summary of the tectonic evolution of western New Guinea and the Banda Arc, showing the major fault zones and structures active over the past 10 My. BHB: Bird’s Head Block; PLFZ: Paniai-Lowlands Fault Zone; SFZ-YFZ: Sorong/Yapen Fault Zone; TAF: Tarera-Aiduna Fault.

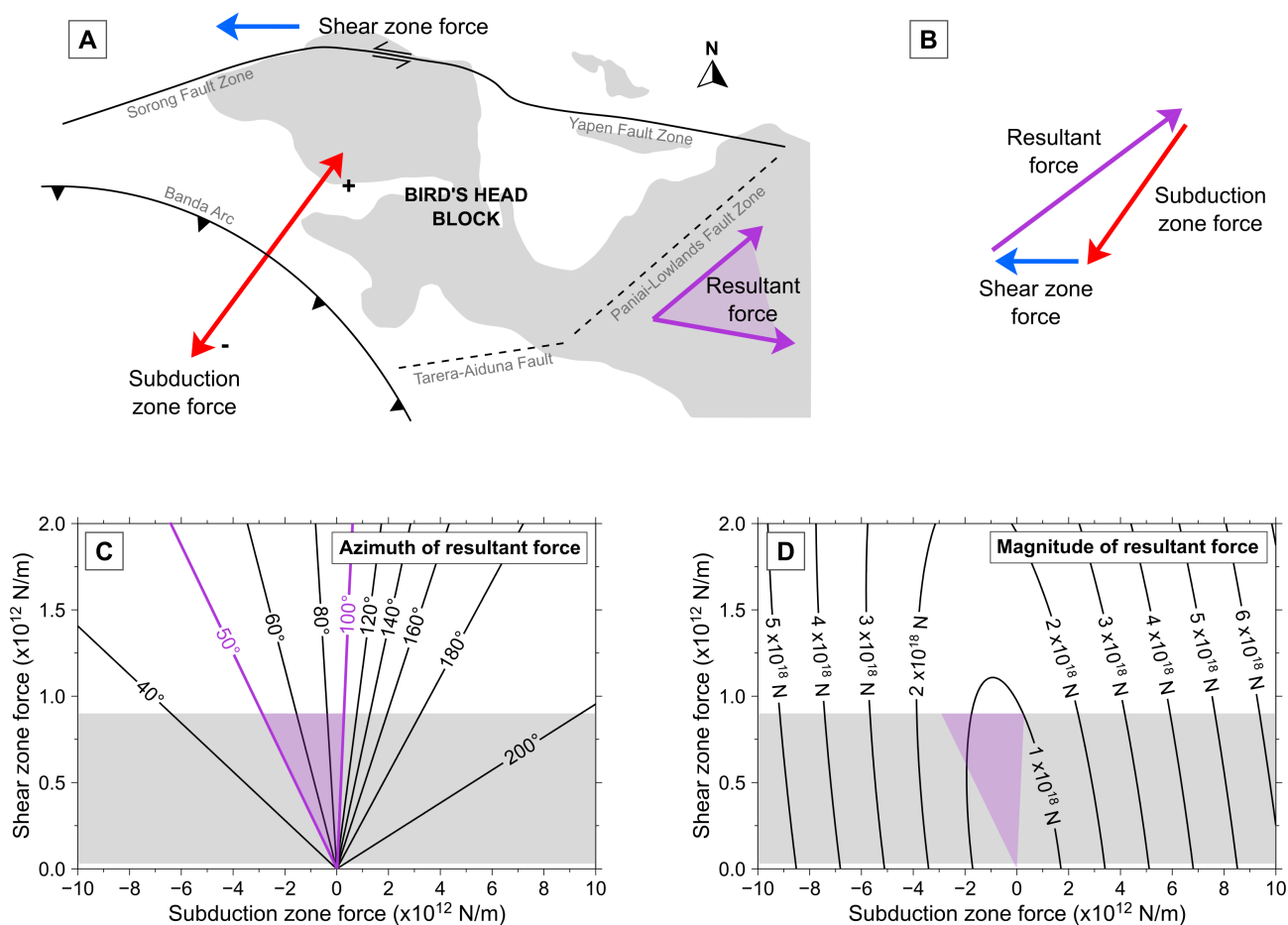


Figure 14: **A:** Cartoon showing the major fault zones acting on the Bird’s Head Block ~ 2 Ma, namely the Banda Arc and the Sorong and Yapen Fault Zones. The + and - symbols next to the subduction zone force indicate the designated positive and negative directions of the force acting from the Banda Arc onto the Bird’s Head Block. The range of possible azimuths of the resultant force (purple shaded region) has been estimated from the slip vectors of earthquakes along the Tarera-Aiduna Fault and Paniai-Lowlands Fault Zone. **B:** Vector summation of the subduction zone force from the Banda Arc and shear zone force from the Sorong and Yapen Fault Zones allows us to estimate the magnitude and azimuth of the resultant force acting on the Bird’s Head Block. **C and D:** Co-varying the magnitude of the subduction and shear zone forces (per metre along-strike) gives estimates of the magnitude and azimuth of the resultant force, plotted as contours. The grey shaded region indicates the plausible values of the shear zone force, and thus the most likely region of parameter space. Our estimate of the azimuth of the resultant force, determined from the slip vectors of recent earthquakes, is indicated by the purple shaded region.